Quark-gluon vertex from $N_f = 2$ lattice QCD

Ayşe Kızılersü,[1] Orlando Oliveira,[2] Paulo J. Silva,[2] Jon-Ivar Skullerud,[3,4,*] and André Sternbeck[5]

[1]*CSSM, Department of Physics, Faculty of Sciences, School of Physical Sciences, University of Adelaide, 5005 Adelaide, Australia*

[2]*CFisUC, Department of Physics, University of Coimbra, 3004–516 Coimbra, Portugal*

[3]*Department of Theoretical Physics, National University of Ireland Maynooth, Maynooth, County Kildare, Ireland*

[4]*School of Mathematics, Trinity College, Dublin 2, Ireland*

[5]*Theoretisch-Physikalisches Institut and Universitätsrechenzentrum, Friedrich-Schiller-Universität Jena, 07743 Jena, Germany*

(Received 15 March 2021; accepted 17 May 2021; published 29 June 2021)

We study the quark-gluon vertex in the limit of vanishing gluon momentum using lattice QCD with two flavors of $\mathcal{O}(a)$ improved Wilson fermions, for several lattice spacings and quark masses. We find that all three form factors in this kinematics have a significant infrared strength and that both the leading form factor λ_1, multiplying the tree-level vertex structure, and the scalar, chiral symmetry breaking form factor λ_3 are significantly enhanced in the infrared compared to the quenched ($N_f = 0$) case. These enhancements are orders of magnitude larger than predicted by one-loop perturbation theory. We find only a weak dependence on the lattice spacing and quark mass.

DOI: 10.1103/PhysRevD.103.114515

I. INTRODUCTION

The quark-gluon vertex is one of the basic building blocks of the strong interaction. It encodes the fundamental interactions of the quarks and gluons and can be used to define a nonperturbative running coupling. In addition, it is an essential ingredient in functional approaches to nonperturbative QCD, such as Dyson-Schwinger equations (DSEs) and the functional renormalization group (FRG). In particular, the DSE for the quark propagator contains the quark-gluon vertex, and the amount of dynamical chiral symmetry breaking is highly sensitive to the details of this vertex; see Ref. [1] for the case of QED.

Traditionally, many studies of hadron phenomenology in the DSE framework have been carried out using the rainbow-ladder truncation, where the quark-gluon vertex is approximated by its tree-level structure, multiplied by an effective coupling which is taken to depend only on the gluon momentum. While this approach has been successful in describing a range of properties of pseudoscalar and vector mesons [2–5], it has failed to provide a satisfactory description of other quantities including scalar and axial-vector mesons and the chiral transition temperature [6–8]. It should also be noted that this approach fails to satisfy the Slavnov-Taylor identities which encode the gauge invariance of QCD.

Through a combination of lattice, DSE, and FRG studies, the elementary (gluon, quark, and ghost) propagators in Landau-gauge QCD are now very well known [9–21], although a continuum extrapolation of lattice results is still outstanding. It is thus natural that attention has in recent years turned to the structure of the three- and four-point vertices of QCD, including the quark-gluon vertex. There have been a number of recent studies within the DSE framework exploring the full structure of this vertex [20,22–35] and the potential impact of the various nonleading form factors on chiral symmetry breaking and hadron phenomenology [24,36–38]. Two critical ingredients in determining the full structure of the vertex have been the Slavnov-Taylor identity, which relates the longitudinal part of the vertex to the quark propagator, and the transverse Ward-Takahashi identities [39–42], which constrain the purely transverse part of the vertex.

The quark-gluon vertex has previously been studied on the lattice in the *quenched approximation* in a series of papers [43–46]. Apart from the uncontrolled systematic uncertainty of the quenched approximation, these studies have only been carried out at a single lattice spacing and volume and hence do not allow for a controlled approach to the physical (continuum and infinite-volume) limit. In this paper, we take the first steps toward rectifying this by computing the quark-gluon vertex on state-of-the-art lattices with $N_f = 2$ light dynamical quarks with different masses and for several lattice spacings and compare with

*jonivar.skullerud@mu.ie

equivalent results in the quenched approximation ($N_f = 0$). Some preliminary findings were presented in Refs. [47,48]. We will conduct this study in the soft gluon kinematics where the gluon momentum is vanishing, and hence both quark momenta are equal.

The structure of this paper is as follows. In Sec. II, we present our methods for computing the vertex, including the notation and vertex decomposition (Sec. II A), lattice simulation details (Sec. II B), procedure for extracting form factors (Sec. II C), and tree-level correction of lattice data (Sec. II D). Our results are presented in Sec. III, while in Sec. IV, we summarize our findings and outline prospects for future work.

II. CONTINUUM AND LATTICE VERTEX

A. Quark-gluon vertex

Our description of the quark-gluon vertex follows the notation used in Refs. [43–45,49,50], which we briefly summarize here.

The proper quark-gluon vertex, $(\Lambda^a_\mu)^{ij}_{\beta\rho} = t^a_{ij}(\Lambda_\mu)_{\beta\rho} = t^a_{ij}(-ig_0\Gamma_\mu)_{\beta\rho}$, is depicted in Fig. 1 with p the outgoing quark momentum, q the outgoing gluon momentum, and $k = p + q$ the incoming quark momentum where t^a_{ij} is the group generator. The quark-gluon vertex can be described in terms of 12 spin amplitudes which would be formed using the three vectors p_μ, q_μ, and γ_μ and four Dirac scalars, I, $\not{p}$, $\not{q}$, and $\not{p}\not{q}$. Reorganizing these spin amplitudes to form a tensor basis, the full one-particle irreducible function $\Lambda^\mu_F(p,q,k)$ can be decomposed into nontransverse and transverse parts,

$$\begin{aligned}\Lambda^\mu_F(p,q,k) &= \Lambda^\mu_{NT}(p,q,k) + \Lambda^\mu_T(p,q,k),\\ &= \sum_{i=1}^{4}\lambda^i(p^2,q^2,k^2)L^\mu_i(p,q,k)\\ &\quad + \sum_{i=1}^{8}\tau^i(p^2,q^2,k^2)T^\mu_i(p,q,k),\end{aligned} \tag{1}$$

where λ^i and $L^\mu_i(p,k,q)$ are nontransverse form factors and basis vectors [51] and τ^i and $T^\mu_i(p,k,q)$ are transverse form factors and basis vectors [52], respectively. By definition, the transverse part is such that $q \cdot T_i(p,k,q) = 0$. In terms of the incoming and outgoing quark momenta, the longitudinal basis can be written as

$$\begin{aligned}L_{1\mu} &= \gamma_\mu,\\ L_{2\mu} &= -(\not{p} + \not{k})(p_\mu + k_\mu),\\ L_{3\mu} &= -i(p_\mu + k_\mu),\\ L_{4\mu} &= -i\sigma_{\mu\nu}(p_\nu + k_\nu).\end{aligned} \tag{2}$$

The nontransverse part of the vertex satisfies the Slavnov-Taylor identity,

$$\begin{aligned}q_\mu\Lambda^\mu(p,q,k) &= q_\mu\Lambda^\mu_{NT}(p,q,k)\\ &= G_h(q^2)[\bar{H}(k,-p,-q)S^{-1}(k)\\ &\quad - S^{-1}(p)H(-p,k,-q)],\end{aligned} \tag{3}$$

which encodes the gauge invariance of the system. Through these Slavnov-Taylor identities, the nontransverse part of the vertex is related to the inverse quark propagator, S^{-1}; the ghost-quark scattering kernel, H; and the ghost dressing function, G_h. However, the transverse part remains unconstrained by the Slavnov-Taylor identity, i.e., $q_\mu\Lambda^\mu_T(p,q) = 0$ and $\Lambda^\mu_T(p,p) = 0$. The transverse basis tensors [52] are given by

$$\begin{aligned}T_{1\mu} &= i[(k\cdot q)p_\mu - (p\cdot q)k_\mu],\\ T_{2\mu} &= (\not{p} + \not{k})[(k\cdot q)p_\mu - (p\cdot q)k_\mu],\\ T_{3\mu} &= \not{q}q_\mu - q^2\gamma_\mu,\\ T_{4\mu} &= -i[q^2\sigma_{\mu\nu}(p_\nu + k_\nu) + 2q_\mu\sigma_{\nu\lambda}p_\nu k_\lambda],\\ T_{5\mu} &= -i\sigma_{\mu\nu}q_\nu,\\ T_{6\mu} &= q\cdot(p+k)\gamma_\mu - \not{q}(p_\mu + k_\mu),\\ T_{7\mu} &= \frac{i}{2}q\cdot(p+k)\sigma_{\mu\nu}(p_\nu + k_\nu) - i(p_\mu + k_\mu)\sigma_{\nu\lambda}p_\nu k_\lambda,\\ T_{8\mu} &= -\gamma_\mu\sigma_{\nu\lambda}p_\nu k_\lambda - \not{p}k_\mu + \not{k}p_\mu,\end{aligned} \tag{4}$$

where $\sigma_{\mu\nu} = \frac{1}{2}[\gamma_\mu,\gamma_\nu]$. Since in this paper we will only consider the soft gluon kinematics where the gluon momentum $q = 0$ and $k = p$, these transverse tensors do not contribute here. The full vertex structure in general kinematics will be considered in a future paper.

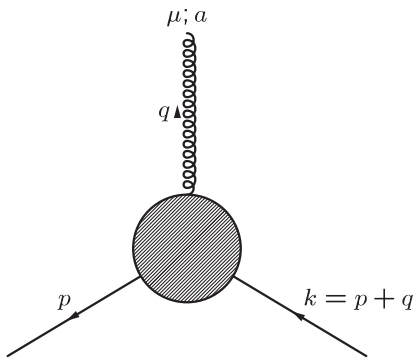

FIG. 1. The proper quark-gluon vertex.

B. Lattice simulation details

In this study, we use the same action and formulation for the quark propagator as in Ref. [16], and refer to that paper and references therein for further details. We employ the Wilson action for the gauge sector and the Sheikholeslami-Wohlert (clover) fermion action [53],

$$S_{\mathrm{SW}} = S_W - i\frac{a}{4}g_0 c_{\mathrm{SW}}\sum_x\sum_{\mu\nu}\bar{\psi}(x)\sigma_{\mu\nu}F_{\mu\nu}(x)\psi(x), \quad (5)$$

where S_W is the ordinary (unimproved) Wilson fermion action. The improvement coefficient c_{SW} has been determined nonperturbatively. In order for the quark propagator and quark-gluon vertex to be fully $\mathcal{O}(a)$ improved, it is also necessary to improve the quark propagator [54], and for this purpose, we use the $\mathcal{O}(a)$ improved "rotated" quark propagator,

$$\begin{aligned} S_R(x,y) &\equiv \langle\psi'(x)\bar{\psi}'(y)\rangle \\ &= \langle\!\langle (1+b_q am)^2(1-c_q a\overrightarrow{\not{D}}(x)) \\ &\quad \times S_0(x,y;U)(1+c_q a\overleftarrow{\not{D}}(y))\rangle\!\rangle, \end{aligned} \quad (6)$$

where the double brackets $\langle\!\langle\cdot\rangle\!\rangle$ denote averaging over gauge fields only, while $S(x,y;U)$ is the quark propagator evaluated on a single gauge configuration U. We use the tree-level values for the coefficients b_q and c_q: $b_q = c_q = 1/4$. We note that this propagator differs from the improved propagator used in Refs. [43–45,49,50].

The quark-gluon vertex is then determined by

$$\Lambda_\mu^{a,\mathrm{lat}}(p,q) = S_R(p)^{-1}V_\nu^a(p,q)S_R(p+q)^{-1}D(q)^{-1}_{\nu\mu}, \quad (7)$$

where the unamputated vertex V is given by

$$V_\mu^a(p,q) = \langle\!\langle S_R(p;U)A_\mu^a(q)\rangle\!\rangle. \quad (8)$$

In Landau gauge, it is not possible to implement Eq. (7) fully since the inverse gluon propagator, $D^{-1}_{\mu\nu}$, does not exist for $q \neq 0$. Instead, we compute the transverse projected vertex

$$\begin{aligned} \tilde{\Lambda}_\mu(p,q) &= -ig_0\tilde{\Gamma}_\mu = P^T_{\mu\nu}(q)\Lambda_\nu(p,q) \\ &= \left(\delta_{\mu\nu} - \frac{q_\mu q_\nu}{q^2}\right)\Lambda_\nu(p,q). \end{aligned} \quad (9)$$

In the present work, we use the same gauge ensembles as in Ref. [16], which are a subset of the gauge ensembles generated by the Regensburg QCD Collaboration (see, e.g., Refs. [55–57]). These ensembles have $N_f = 2$ dynamical quarks with pion masses in the range 280–420 MeV. Three values of the lattice spacing, $a \approx 0.081$ fm, $a \approx 0.071$ fm, and $a \approx 0.060$ fm, are used. Most of the calculations have been carried out on a lattice volume of $32^3 \times 64$, but we have also used a 64^4 lattice to check finite-volume effects for one of the parameter choices ($m_\pi \approx 290$ MeV).

In addition, we have produced a quenched ensemble with lattice spacing matching that of ensembles L07 and H07, i.e., with $a = 0.07$ fm, but with a larger valence quark mass $m_\pi \approx 1000$ MeV.

The parameters used are listed in Table I. In order to more easily refer to the different ensembles when presenting the results, we have labeled them such that the first letter refers to the pion mass [heavy (H), 420 MeV, or light (L), 290 MeV], and the following two digits refer to the lattice spacing. The quenched ensemble is labeled Q07.

For the gauge fixing, we used an over-relaxation algorithm which iteratively maximizes the Landau-gauge functional

$$F_U[g] = \frac{1}{4V}\sum_{x\mu}\mathrm{ReTr}U^g_{x\mu}, \quad (10)$$

with $U^g_{x\mu} = g_x U_{x\mu} g^\dagger_{x+\hat{\mu}}$ and $g_x \in SU(3)$. As stopping criterion, we used

$$\max_x \mathrm{ReTr}[(\nabla_\mu A_{x\mu})(\nabla_\mu A_{x\mu})^\dagger] < 10^{-9}, \quad (11)$$

where $A_{x\mu} \equiv \frac{1}{2iag_0}(U^g_{x\mu} - U^{g\dagger}_{x\mu})|_{\mathrm{traceless}}$ and $\nabla_\mu A_{x\mu} \equiv \sum_\mu (A_{x\mu} - A_{x-\hat{\mu},\mu})$, as usual.

C. Form factor extraction

In the soft gluon kinematics ($q_\mu = 0$, $k_\mu = p_\mu$), the continuum vertex is given by the three nontransverse form factors λ_1, λ_2, and λ_3 [58],

$$\begin{aligned} (\tilde{\Lambda}^a_\mu)^{ij}_{\alpha\beta} &= t^a_{ij}(\bar{\Lambda}_\mu)_{\alpha\beta} \\ &= -ig_0 t^a_{ij}(\lambda_1[\gamma_\mu] + \lambda_2[-4\not{p}p_\mu] + \lambda_3[-2ip_\mu])_{\alpha\beta}. \end{aligned} \quad (12)$$

TABLE I. Lattice parameters used in this study. The lattice spacings a and pion masses m_π and critical hopping parameters used to obtain the subtracted bare quark mass $m_q = 1/(2\kappa) - 1/(2\kappa_c)$ are all taken from Ref. [56]. The quenched ensemble Q07 was produced specifically for this study. N_{src} denotes the number of different point sources per configuration used to produce the quark propagators.

Name	β	κ	a (fm)	V	m_π (MeV)	m_q (MeV)	N_{cfg}	N_{src}
L08	5.20	0.13596	0.081	$32^3 \times 64$	280	6.2	900	4
H07	5.29	0.13620	0.071	$32^3 \times 64$	422	17.0	900	4
L07	5.29	0.13632	0.071	$32^3 \times 64$	295	8.0	908	4
L07-64	5.29	0.13632	0.071	$64^3 \times 64$	290	8.0	750	2
H06	5.40	0.13647	0.060	$32^3 \times 64$	426	18.4	900	4
Q07	6.16	0.1340	0.071	$32^3 \times 64$	1000	130	998	4

We can extract these individual form factors by taking appropriate contractions and traces,

$$\mathrm{Tr}_4[I(\bar{\Lambda}^a_\mu)] = -ig_0(\lambda_3[-2ip_\mu]), \tag{13}$$

$$\mathrm{Tr}_4[\gamma_\nu(\bar{\Lambda}^a_\mu)] = -ig_0(\lambda_1\delta_{\nu\mu} + \lambda_2[-4p_\nu p_\mu]), \tag{14}$$

where $\mathrm{Tr}_4 \equiv \frac{\mathrm{Tr}}{4}$ denotes the trace over spin indices. We note that Eq. (14) implies that λ_1 and λ_2 are coupled, but we can disentangle them by contracting it with the tensors $\delta_{\mu\nu}$ and $p_\mu p_\nu$ and solving the coupled equations. This yields the following expressions:

$$\lambda_1 = \frac{1}{(-ig_0)}\left\{\frac{1}{3}\left[\mathrm{Tr}_4(\gamma_\mu\bar{\Lambda}_\mu) - \frac{p_\mu p_\nu}{p^2}\mathrm{Tr}_4(\gamma_\nu\bar{\Lambda}_\mu)\right]\right\}, \tag{15}$$

$$\lambda_2 = \frac{1}{(-ig_0)}\left\{\frac{1}{12p^2}\left[\mathrm{Tr}_4(\gamma_\mu\bar{\Lambda}_\mu) - 4\frac{p_\mu p_\nu}{p^2}\mathrm{Tr}_4(\gamma_\nu\bar{\Lambda}_\mu)\right]\right\}, \tag{16}$$

$$\lambda_3 = \frac{1}{(-ig_0)}\left\{\frac{i}{2}\frac{p_\mu}{p^2}\mathrm{Tr}_4(I\bar{\Lambda}_\mu)\right\}. \tag{17}$$

In practice, expressions such as Eqs (15) and (16) contain multiple terms that can lead to numerically poorly determined form factors. It may therefore be desirable to sacrifice covariance and restrict ourselves to specific momentum configurations in order to obtain simple expressions involving only a single term. For instance, with the choices of (a) $\nu = \mu$ and $p_\mu = 0$ and (b) $\nu \neq \mu$ in Eq. (14), we obtain the following noncovariant, single term expressions for the continuum λ_1 and λ_2 form factors, respectively, which we will make use of in this analysis:

$$\lambda_1 = \frac{1}{(-ig_0)}\left\{[\mathrm{Tr}_4(\gamma_\alpha\bar{\Lambda}_\mu)]|_{\substack{\alpha=\mu \\ p_\mu=0}}\right\}, \tag{18}$$

$$\lambda_2 = \frac{1}{(-ig_0)}\left\{-\frac{1}{4p^2}\frac{p_\alpha p_\mu}{p^2}[\mathrm{Tr}_4(\gamma_\alpha\bar{\Lambda}_\mu)|_{\alpha\neq\mu}]\right\}, \tag{19}$$

The quark-gluon vertex computed on the lattice using Eq. (7) is not renormalized. To renormalize the vertex, we impose a momentum subtraction scheme whereby the leading form factor λ_1 takes on its tree-level value at a given renormalization scale μ,

$$\lambda_1^R(\mu^2, 0, \mu^2) = 1. \tag{20}$$

This fixes the renormalization constant Z_1 such that $\Gamma^{\mathrm{lat}}_\mu(p,q,k) = Z_1\Gamma^R_\mu(p,q,k)$, which in turn determines the renormalization of all the form factors.

D. Tree-level correction

In order to determine the lattice equivalents of the continuum expressions (18), (19), and (17) for the form factors λ_1, λ_2, and λ_3 and to estimate and reduce their lattice artifacts, we need to compute the structure of the lattice tree-level vertex. Here, we will outline the main results, while the details are given in the Appendix.

The tree-level quark-gluon vertex associated with the Sheikholeslami-Wohlert action without color and group indices is given by [59,60]

$$\begin{aligned}\bar{\Lambda}^{(0)}_{0,\nu}(p,q,k) = (-ig_0)\Bigg\{&\boldsymbol{\gamma}_\nu\cos\left(\frac{a(p_\nu+k_\nu)}{2}\right)\\ &- i\sin\left(\frac{a(p_\nu+k_\nu)}{2}\right)\boldsymbol{I}\\ &- i\frac{c_{\mathrm{SW}}}{2}\cos\left(\frac{aq_\nu}{2}\right)\sum_\lambda\boldsymbol{\sigma_{\nu\lambda}}\sin(aq_\lambda)\Bigg\},\end{aligned} \tag{21}$$

for the case of the "unimproved" propagator $S_0(x,y) = \langle\psi(x)\bar{\psi}(y)\rangle$. The improved vertex obtained using the rotated propagator of Eq. (6) is given at tree level by

$$\begin{aligned}\bar{\Lambda}^{(0)}_{R,\mu}(p,q,k) = (1+b_q am)[S^{(0)}_R(p)]^{-1}&S^{(0)}_0(p)[\Lambda^{a(0)}_{0,\mu}(p,q,k)]\\ &\times S^{(0)}_0(k)[S^{(0)}_R(k)]^{-1},\end{aligned} \tag{22}$$

where $S^{(0)}_0(p)$ is the tree-level unimproved dimensionless Wilson quark propagator, while $S^{(0)}_R(p)$ is the level expression for the improved propagator of Eq. (6). In the soft gluon kinematics with $q = 0$, $p = k$, this reduces to

$$\begin{aligned}\bar{\Lambda}^{(0)}_{R,\mu}(p,0,p) = (-ig_0)&\frac{(1+b_q am)}{(1+am/2)^2}\frac{1}{(1+c_q^2a^2K^2(p))^4}\\ &\times\Bigg\{\boldsymbol{\gamma_\mu}[(1+c_q^2a^2K^2(p))^2C_\mu(p)]\\ &-\boldsymbol{4a^2K_\mu \not{K}(p)}[2c_q^2C_\mu(p) - c_q(1-c_q^2a^2K^2(p))]\\ &-\boldsymbol{2iaK_\mu}\Bigg[-2c_q^2a^2K^2(p) + \frac{1}{2}(1-c_q^2a^2K^2(p))\\ &-2c_q(1-c_q^2a^2K^2(p))C_\mu(p)\Bigg]\Bigg\},\end{aligned} \tag{23}$$

where we have defined the lattice momentum variables

$$K_\mu(p) = \frac{1}{a}\sin(p_\mu a), \qquad C_\mu(p) = \cos(p_\mu a). \tag{24}$$

We note in particular that there are two separate tensor structures appearing in the tree-level vertex (23), which in the continuum become equal to $L_{2,\mu}$, and likewise for $L_{3,\mu}$. In Eqs (29) and (30) below, these are associated with separate form factors $\lambda^{(0)}_i$ and $\bar{\lambda}^{(0)}_i$, respectively. It should be noted that all of these are proportional to the lattice spacing a and hence vanish in the naive continuum limit, and

likewise the deviation between $\lambda_1^{(0)}$ and the continuum, tree-level value of 1 vanishes in the same limit. However, their magnitude can be large at finite lattice spacing.

Due to asymptotic freedom, we expect the nonperturbative vertex to approach its tree-level form at large momentum and hence be dominated by lattice artifacts. We attempt to reduce these by dividing the lattice λ_1 by its tree-level form, while subtracting off the tree-level expression from the raw data for λ_2 and λ_3.

Making a comparison between Eq. (23) and the continuum vertex Eq. (12), we end up with the tree-level corrected, lattice equivalents of the expressions (18), (19), and (17),

$$\lambda_1(p^2,0,p^2) = \frac{\mathbf{Im}}{g_0}\left\{[\mathrm{Tr}_4(\gamma_\alpha \bar{\Lambda}_\mu)]|_{\substack{\alpha=\mu \\ p_\mu=0}}\right\}\Big/\lambda_1^{(0)} \tag{25}$$

$$\lambda_2(p^2,0,p^2) = \frac{\mathbf{Im}}{g_0}\left\{-\frac{1}{4K(p)^2}\frac{K_\alpha(p)K_\mu(p)}{K(p)^2}[\mathrm{Tr}_4(\gamma_\alpha \bar{\Lambda}_\mu)|_{\alpha\neq\mu}]\right\} - (\lambda_2^{(0)} + \bar{\lambda}_{2(\mu)}^{(0)}), \tag{26}$$

$$\lambda_3(p^2,0,p^2) = \frac{\mathbf{Re}}{(-g_0)}\left\{\frac{1}{2}\frac{K_\mu(p)}{K^2(p)}\mathrm{Tr}_4(I\bar{\Lambda}_\mu)\right\} - (\lambda_3^{(0)} + \bar{\lambda}_{3(\mu)}^{(0)}), \tag{27}$$

where the lattice tree-level form factors are given by

$$\lambda_1^{(0)} = F(p)(1 + c_q^2 a^2 K^2(p))^2, \tag{28}$$

$$\lambda_2^{(0)} + \bar{\lambda}_{2(\mu)}^{(0)} = a^2 F(p)[-c_q(1 - c_q^2 a^2 K^2(p)) + 2c_q^2 C_\mu(p)], \tag{29}$$

$$\lambda_3^{(0)} + \bar{\lambda}_{3,(\mu)}^{(0)} = \frac{a}{2}F(p)[(1 - c_q^2 a^2 K^2(p))^2 - 4c_q^2 a^2 K^2(p) - 4c_q(1 - c_q^2 a^2 K^2(p))C_\mu(p)] \tag{30}$$

and the common prefactor $F(p)$ is given by

$$F(p) = \frac{(1 + b_q am)}{(1 + am/2)^2}\frac{1}{(1 + c_q^2 a^2 K^2(p))^4}. \tag{31}$$

These $(\lambda_1, \lambda_2, \lambda_3)$ are the complete form factors required to determine the quark-gluon vertex in the soft gluon limit, and Eqs (25), (26), and (27) define the exact procedures to calculate them on the lattice.

E. One-loop continuum form factors

In interpreting the lattice data for the various quark-gluon vertex form factors, knowledge of the corresponding perturbative expressions will be useful. Therefore, for completeness, we report on the results for the Landau gauge one-loop Euclidean-space form factors $\lambda_{1,2,3}$ in the soft gluon kinematics in the momentum subtraction (MOM) scheme, where μ is the renormalization scale, see Fig. 2.

$$\lambda_1^{\mathrm{pert}}(p^2,0,p^2;\mu^2) = 1 - \frac{\alpha_\mu}{4\pi}\frac{C_A}{4}\left(-\frac{m^2}{p^2} + \frac{m^2}{\mu^2} - 3\ln\left(\frac{p^2+m^2}{\mu^2+m^2}\right) + \frac{m^4}{p^4}\ln\left(1+\frac{p^2}{m^2}\right) - \frac{m^4}{\mu^4}\ln\left(1+\frac{\mu^2}{m^2}\right)\right) + \mathcal{O}(\alpha^2), \tag{32}$$

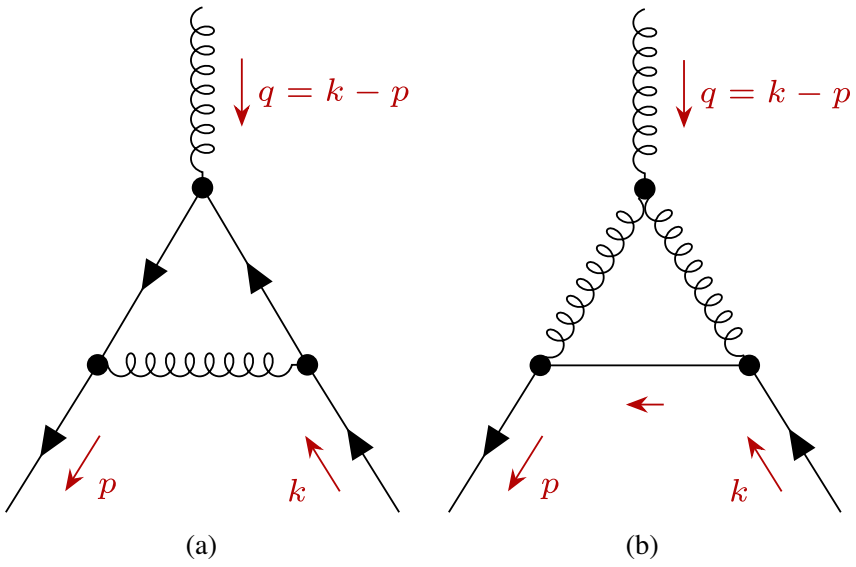

FIG. 2. Complete one-loop diagrams of the quark-gluon vertex. (a) Abelian contribution. (b) Non-abelian contribution

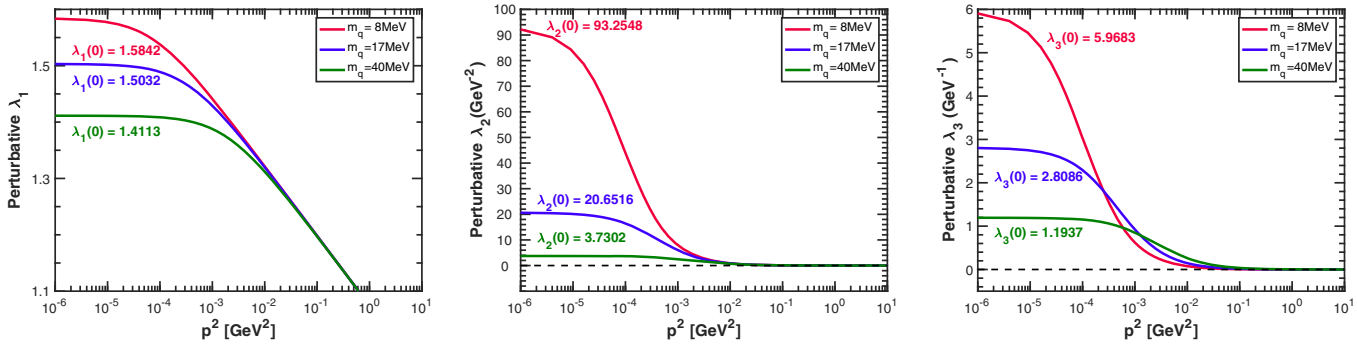

(a) λ_1. (b) λ_2. (c) λ_3.

FIG. 3. One-loop perturbative form factors of the quark-gluon vertex.

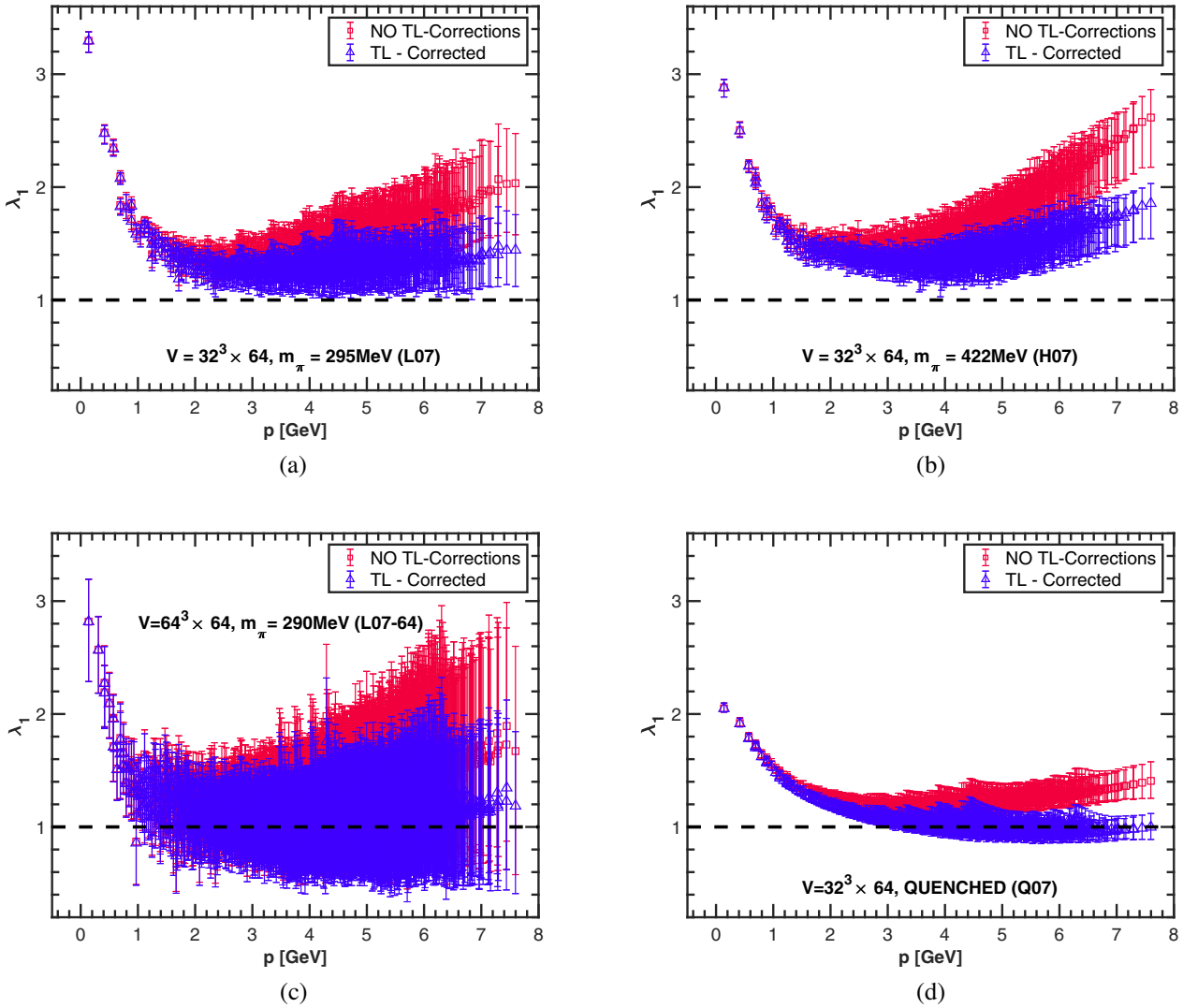

(a) (b) (c) (d)

FIG. 4. The leading, unrenormalized form factor $\lambda_1(p^2, 0, p^2)$ with and without tree-level (TL) corrections as a function of momentum p, for different lattice ensembles with $a = 0.07$ fm: (a) L07, (b) H07, (c) L07-64, and (d) Q07.

$$\lambda_2^{\text{pert}}(p^2,0,p^2) = \frac{\alpha_\mu}{4\pi}\frac{C_A}{8p^2}\left(1 - 2\frac{m^2}{p^2} + 2\frac{m^4}{p^4}\ln\left(1+\frac{p^2}{m^2}\right)\right) + \mathcal{O}(\alpha^2), \tag{33}$$

$$\lambda_3^{\text{pert}}(p^2,0,p^2) = \frac{\alpha_\mu}{4\pi}3C_F\frac{m}{p^2}\left(1 - \frac{m^2}{p^2}\ln\left(1+\frac{p^2}{m^2}\right)\right) + \mathcal{O}(\alpha^2). \tag{34}$$

C_A and C_F are the eigenvalues of the quadratic Casimir operator in the fundamental representation and adjoint representation, respectively: $C_A = N$, $C_F = N^2 - 1/2N$, with $N = 3$ for SU(3). Note that λ_3 is proportional to the quark mass and a nonvanishing λ_3, as is observed in lattice simulations, is an indication of chiral symmetry breaking.

The one-loop expressions are plotted in Fig. 3, for three different values of the quark mass. The value of the form factors in the limit $p \to 0$ is also shown in the graph. We note that all three form factors are enhanced in the infrared and that this enhancement increases with decreasing quark mass for all three. This has also been observed in other kinematics [29]. In the case of λ_3, however, we note that this mass ordering only occurs in the very far infrared, $p \lesssim 15$ MeV, and that the mass ordering is the opposite for $p \gtrsim 50$ MeV, which includes all momenta available for the lattice volumes considered in this study.

III. RESULTS

In the following, we will present our results for the quark-gluon vertex in such a way as to carefully trace the effects of tree-level correction (Sec. III A), unquenching (Sec. III B), mass (Sec. III C), volume (Sec. III D), and lattice spacing (Sec. III E) on each of the three form factors.

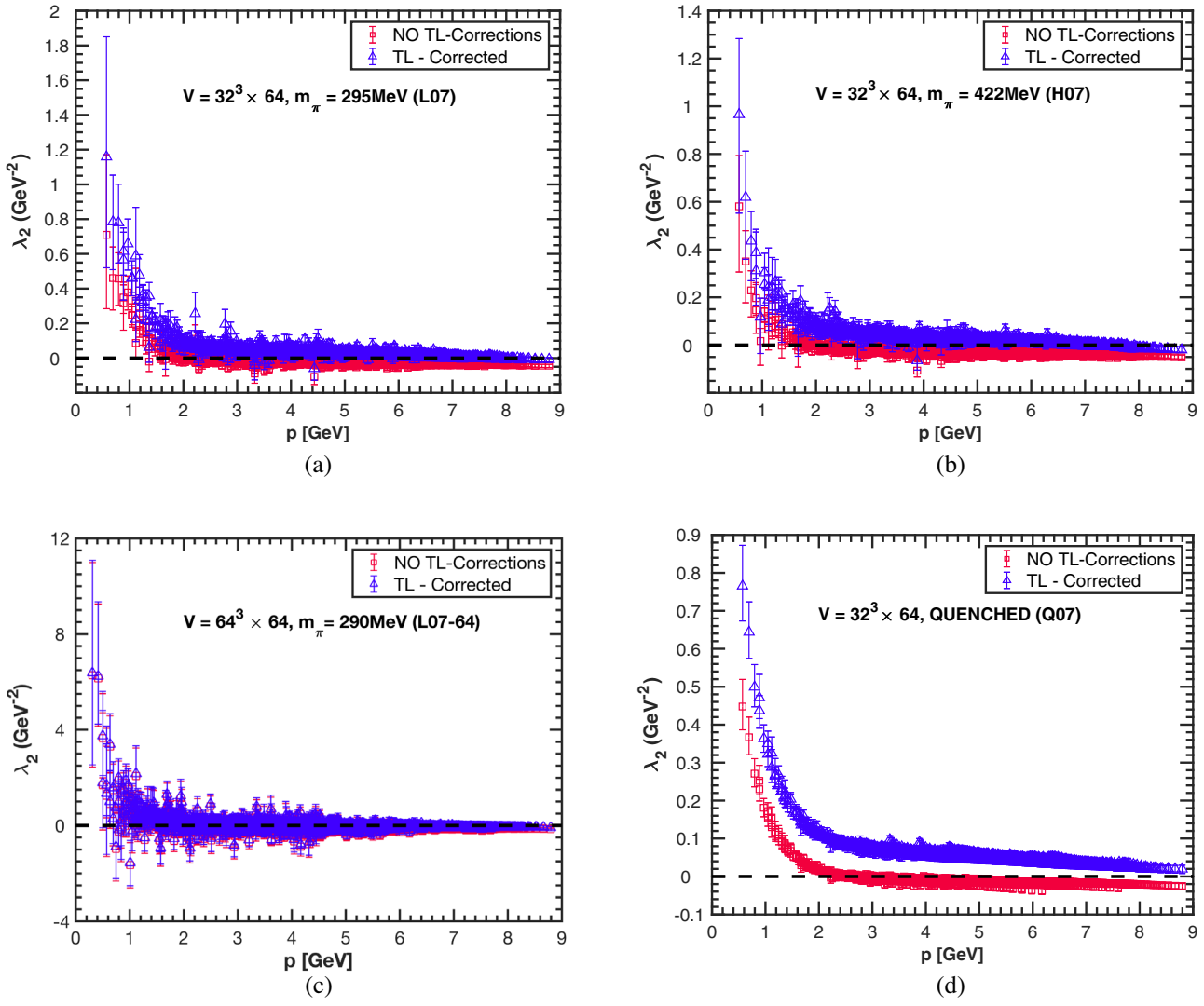

FIG. 5. As in Fig. 4, for the unrenormalized form factor λ_2.

A. Tree-level corrected versus uncorrected

We first consider the effect of the tree-level corrections on the vertex, starting with the leading vertex component λ_1. Representative results for λ_1 as a function of momentum p with and without tree-level correction are shown in Fig. 4. Figure 4(d) shows quenched results, $N_f = 0$, while Figs. 4(a) and 4(c) show results for $a = 0.07$ fm and $m_\pi \simeq 295$ MeV on the $32^3 \times 64$ and $64^3 \times 64$ lattices, respectively. For comparison, Fig. 4(b) shows the results for the heavier pion mass, $m_\pi = 422$ MeV.

Due to asymptotic freedom, we expect that $\lambda_1(p) \to 1$ (plus logarithmic corrections) at large p, and we can see that the tree-level corrections have the effect of bringing the lattice data closer to this continuumlike form for all cases and reducing the violations of rotational symmetry compared to the uncorrected data. In some cases (notably for the largest quark mass $m_\pi = 422$ MeV), we see indications that significant lattice artifacts remain even after tree-level correction and, therefore, careful study of the lattice spacing dependence will be necessary to determine the large-momentum behavior of the vertex. For the larger volume ($64^3 \times 64$), the fluctuations of λ_1 are quite large, Fig. 4(c). In all cases, the tree-level correction is small below 1 GeV but becomes pronounced for $p \gtrsim 1$ GeV ($pa \gtrsim 0.4$).

Using the same lattice ensembles as in Fig. 4, the effect of the tree-level corrections on the λ_2 are shown in Fig. 5. We see that λ_2 tends to zero as p increases, in contrast to λ_1, which approaches a value close to 1—in line with expectations from asymptotic freedom in both cases. On the larger volume $64^3 \times 64$ lattice, the tree-level correction does not appear to have any effect on the λ_2 lattice artifacts within the uncertainties of the data. However, the different vertical scales complicate the comparison with the other figures. The response of the λ_2 to tree-level corrections is noticeable for all momenta. The data in Fig. 5 also

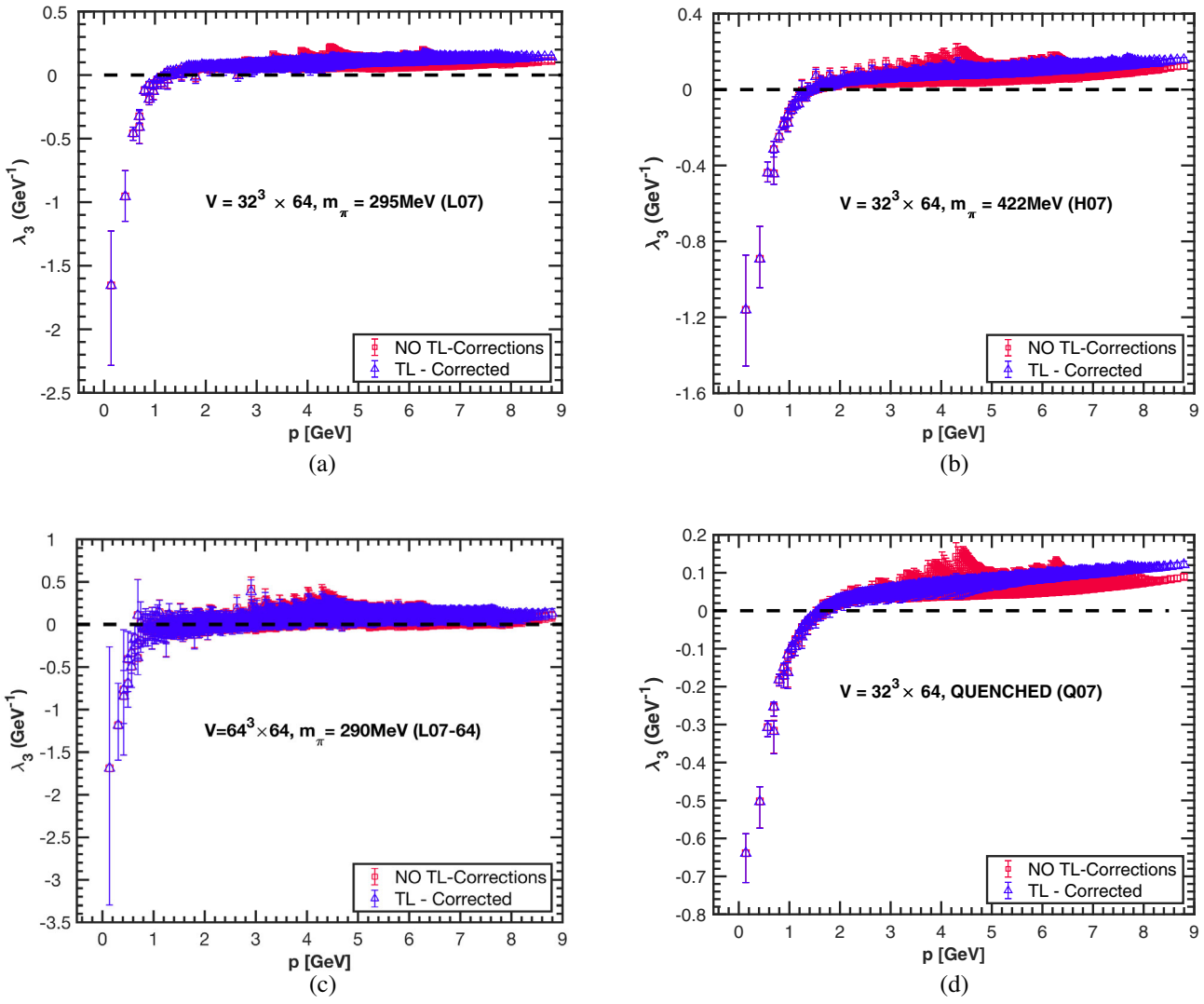

FIG. 6. As in Fig. 4, for the unrenormalized form factor λ_3.

show that λ_2 is strongly enhanced at low momenta, although the volume and mass dependence of λ_2 are difficult to disentangle. The data also suggest that λ_2 is enhanced for dynamical simulations relative to the quenched case.

In Fig. 6, the effect of the tree-level corrections on λ_3 are shown. They are pronounced at large momentum of around 2 GeV onward and have almost no effect for momenta less than 2 GeV. The corrections pushes λ_3 upward in the ultraviolet, and λ_3 does not vanish at higher momenta as one would expect. This appears to be the case for all ensembles. We conclude that in the case of λ_3 the tree-level correction does not work satisfactorily for $pa \gtrsim 1.5$, corresponding to momenta greater than approximately 4 GeV, and we will discard our results for $pa \gtrsim 1.5$ ($p \gtrsim 4$ GeV) as unreliable in the absence of a careful, controlled continuum extrapolation.

The results for all our ensembles are collated in Figs. 7. This figure shows only minor variations with the quark mass and lattice spacing, with indications that decreasing the quark mass leads to a slightly stronger enhancement in the infrared, while decreasing the lattice spacing may have a small effect in the same direction. Indeed, for all form factors, we see that their magnitude is largest for the H06 ensemble ($m_\pi = 426$ MeV, $a = 0.06$ fm). We will discuss the quark mass and lattice spacing dependence in more detail in Secs. III C and III E.

The most striking feature of λ_2 in Fig. 7(b) is that this form factor appears to diverge more strongly in the infrared as we approach the continuum limit. Our results for λ_3 are summarized in Fig. 7(c). We find that the magnitude of λ_3 in the infrared increases with increasing quark mass, which is expected since, according to perturbation theory, this form factor breaks chiral symmetry and is proportional to

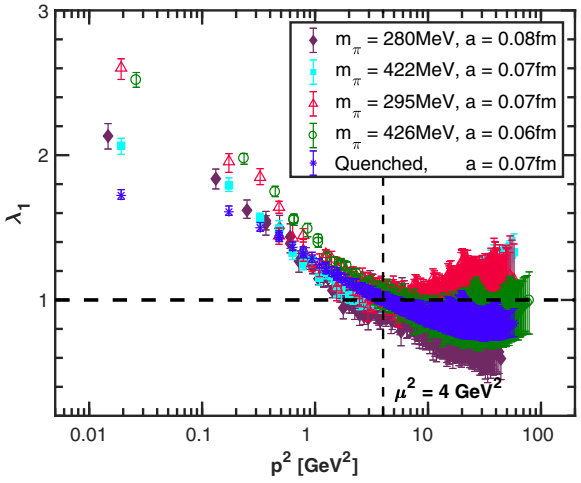

(a) λ_1

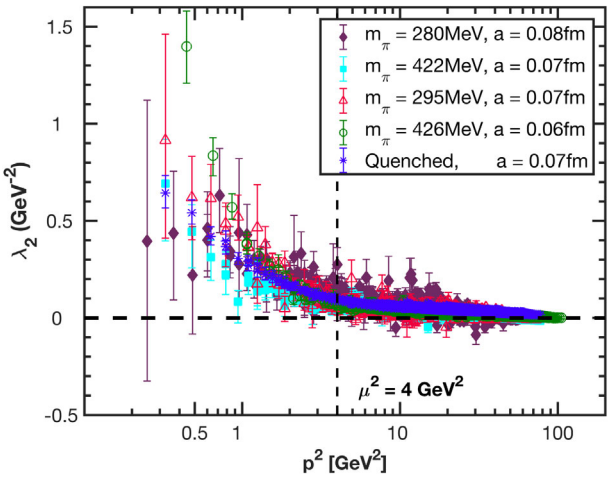

(b) λ_2.

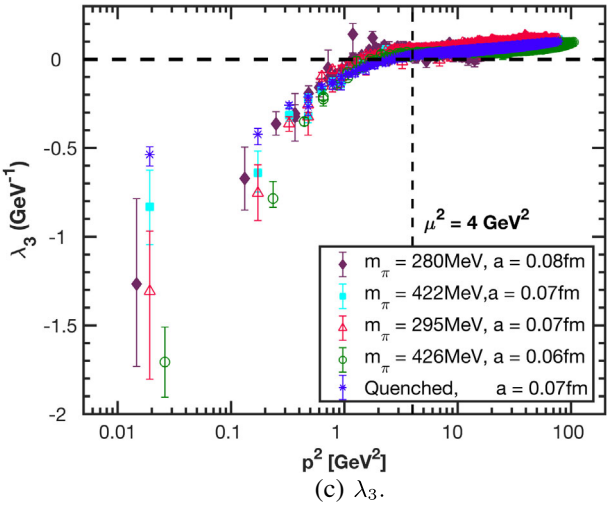

(c) λ_3.

FIG. 7. The form factors λ_1, λ_2, and λ_3 with tree-level corrections versus momentum p^2. All form factors have been renormalized at 2 GeV.

the quark mass, Eq. (34). Our result also suggest that its infrared magnitude increases as we approach the continuum limit.

From now on, we will only show tree-level corrected data. All data shown from here on have been renormalized at 2 GeV, and to make the presentation clearer, we have averaged data with nearby values of momentum, with a momentum bin size $a\Delta p = 0.05$.

B. Quenched versus dynamical

We now turn to a comparison of results from our quenched ($N_f = 0$) and dynamical ($N_f = 2$) ensembles at $a = 0.07$ fm. Since the valence quark mass in the quenched case is quite large, we use the H07 ($m_\pi = 422$ MeV) ensemble in this comparison. The results are shown in Fig. 8. The one-loop perturbative expression (32), evaluated at $\alpha = 0.3 \approx \alpha_{\overline{\rm MS}}(2\ {\rm GeV})$ [61,62] and $m_q = 17$ MeV and with $\mu = 2$ GeV, is also plotted. We have used the subtracted bare quark mass rather than the renormalized mass in this calculation, but this makes little difference as varying m_q even by a factor 2 has a negligible effect for the range of momenta we are considering here.

We will now discuss each form factor in turn.

(i) λ_1: Although we find that the qualitative behavior is the same in both quenched and unquenched cases, we see that with dynamical fermions the vertex is more strongly infrared enhanced than in the quenched case, as seen in Fig. 8(a). However, a more detailed comparison, with different valence quark masses, will be required to disentangle the effects of dynamical fermions and valence quark masses. Even at one-loop order, the perturbative contribution to λ_1 shows IR enhancement, and at one-loop level in Landau gauge, this is purely due to the non-Abelian contribution.

(ii) λ_2: This form factor has a large uncertainty in the IR, and as the momentum increases, its value

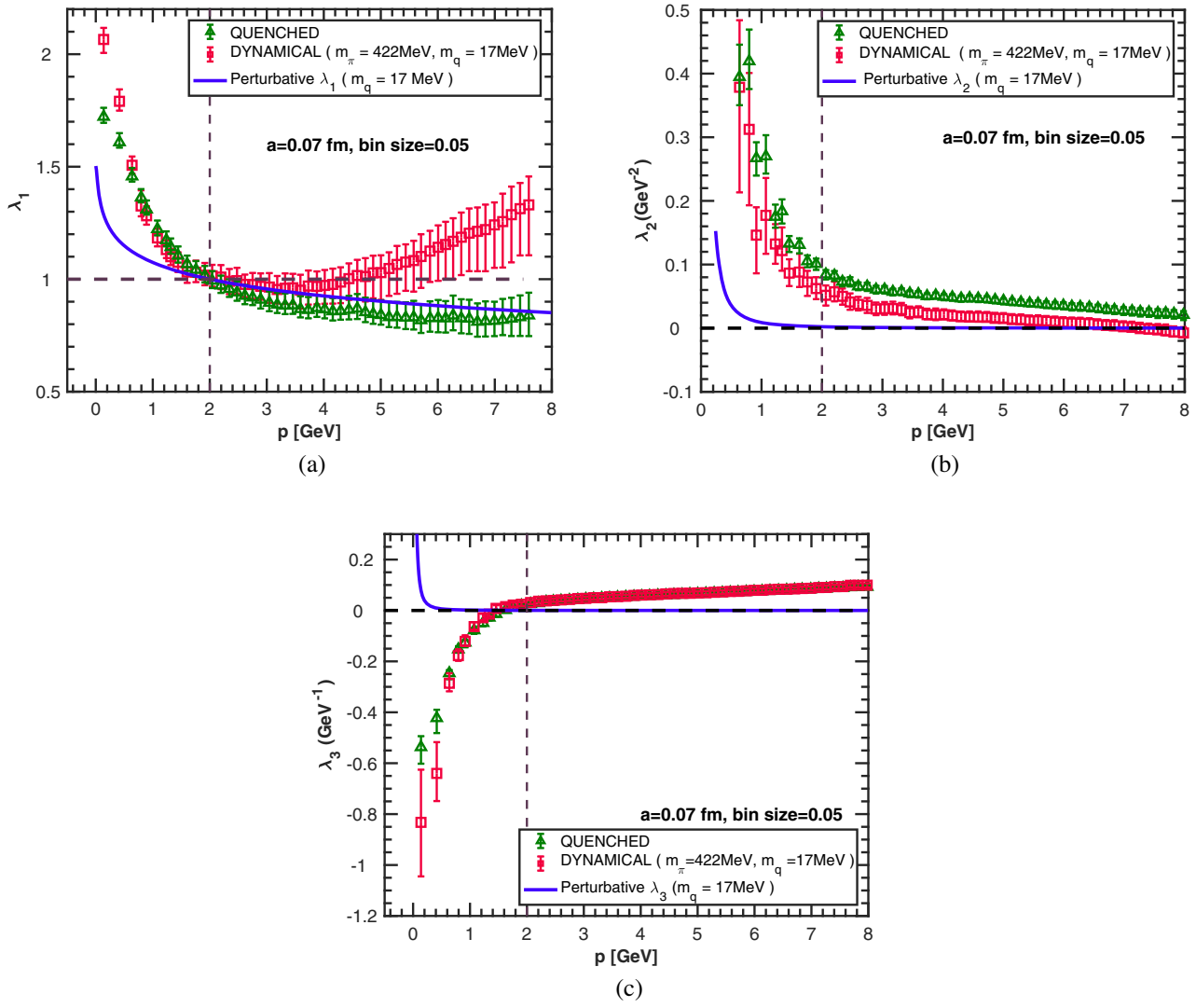

FIG. 8. Quenched and dynamical form factors vs momentum p.

approaches zero, and the uncertainties become small [see Fig. 8(b)]. Here, we clearly see that the dynamical quarks only have a small effect on this form factor, leading at most to a slight enhancement. We also note that our lattice results λ_2 are orders of magnitude larger than the one-loop perturbative expression, which only exhibits a very small increase in the deep infrared. Like in λ_1, the entire contribution in Landau gauge to λ_2 at one-loop level is purely non-Abelian.

(iii) λ_3: As was the case for λ_1, we find that inclusion of dynamical fermions leads to a significant enhancement of this form factor in the infrared; however, above 1 GeV, the difference between dynamical and quenched fermions diminishes. At lower momentum, this form factor is negative, and as the momentum increases, it approaches zero. We find a zero crossing between 1 and 2 GeV. We note that at this point, the uncertainties associated with the tree-level correction are not yet significant, so it appears unlikely that this zero crossing is entirely due to lattice artifacts. The one-loop expression has contributions from both Abelian and non-Abelian diagrams, and the combined effect is positive in the IR region, in contrast to what is found from the lattice data. Since we expect the perturbative behavior to be reproduced at large momentum, this suggests that λ_3 should approach zero from above in the ultraviolet and hence have a zero crossing in the intermediate-momentum region.

Figure 9 shows results for all three form factors for the H07 (dynamical) and Q07 (quenched) ensembles, along with the Abelian Ball-Chiu vertex [51] and the one-loop

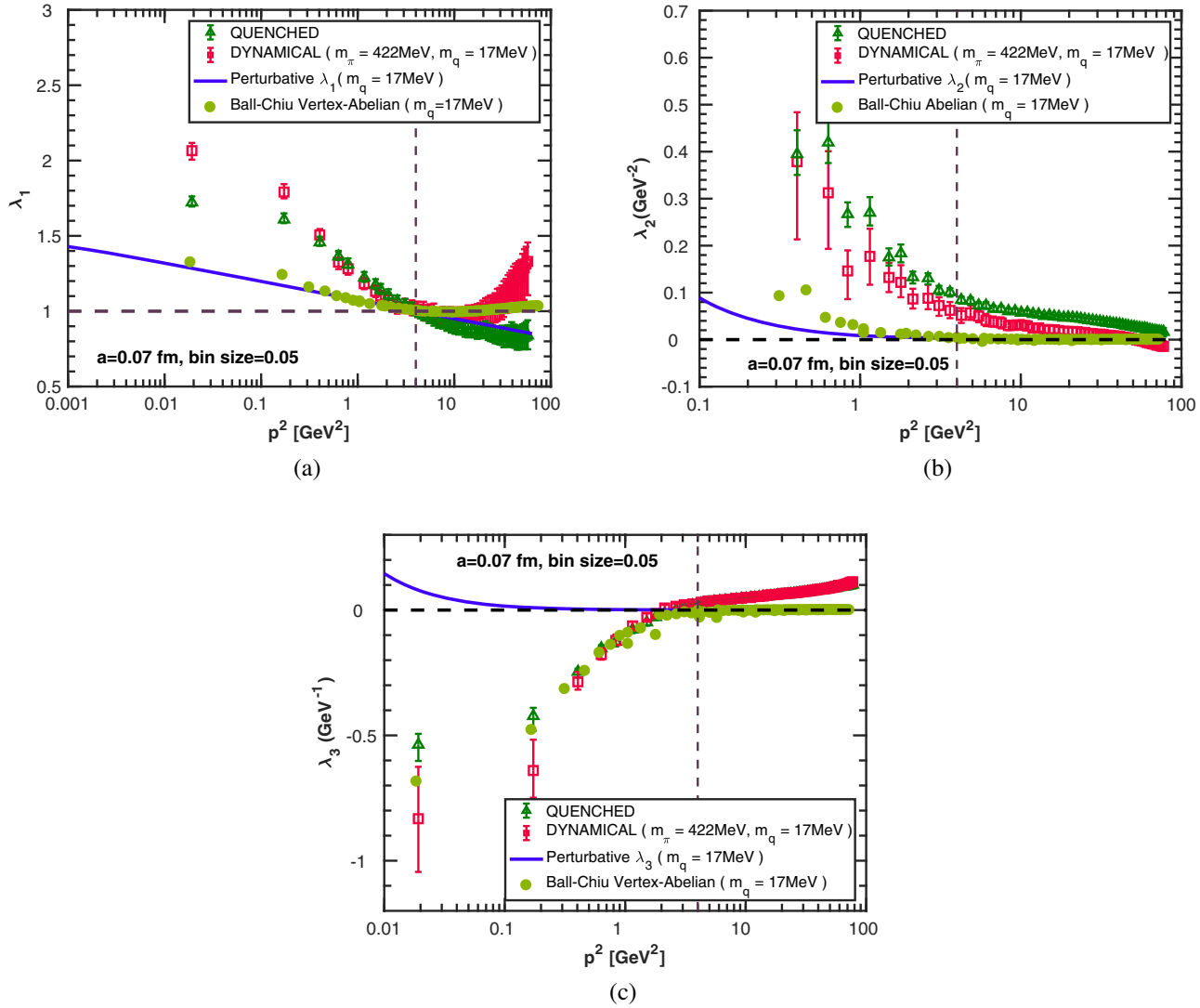

FIG. 9. The form factors λ_1, λ_2, and λ_3 for quenched and dynamical fermions, renormalized at 2 GeV, the Abelian Ball-Chiu vertex, and the one-loop order form factors as functions of momentum squared.

perturbative contributions to the quark-gluon vertex. The Ball-Chiu vertex is calculated from the quark propagator

$$S(p) = \frac{1}{i\not{p}A(p^2) + B(p^2)} = \frac{Z(p^2)}{i\not{p} + M(p^2)}, \quad (35)$$

using the expressions

$$\lambda_1^{BC} = A(p^2), \quad (36)$$

$$\lambda_2^{BC} = -\frac{1}{2} dA(p^2)/dp^2, \quad (37)$$

$$\lambda_3^{BC} = dB(p^2)/dp^2. \quad (38)$$

The quark wave function $A(p^2) = 1/Z(p^2)$ and the mass function $M(p^2) = B(p^2)/A(p^2)$ are calculated using the $N_f = 2$ lattice results from Ref. [16].

We observe a hierarchy in the infrared enhancement of λ_1 where the largest enhancement is for the dynamical lattice ensembles, followed by the quenched lattice data, the Ball-Chiu vertex, and the one-loop perturbative expression in that order. The same hierarchy is found for λ_2, while for λ_3, the quenched and dynamical lattice results and the Ball-Chiu are roughly equal. More work will be required to disentangle the effects of explicit and spontaneous chiral symmetry breaking and quark dynamics in this form factor. We will study the quark mass dependence of λ_3 further in Sec. III C.

The IR hierarchy casts light on the reliability of the various approximations when they are used to calculate nonperturbative quantities. These results combined with the

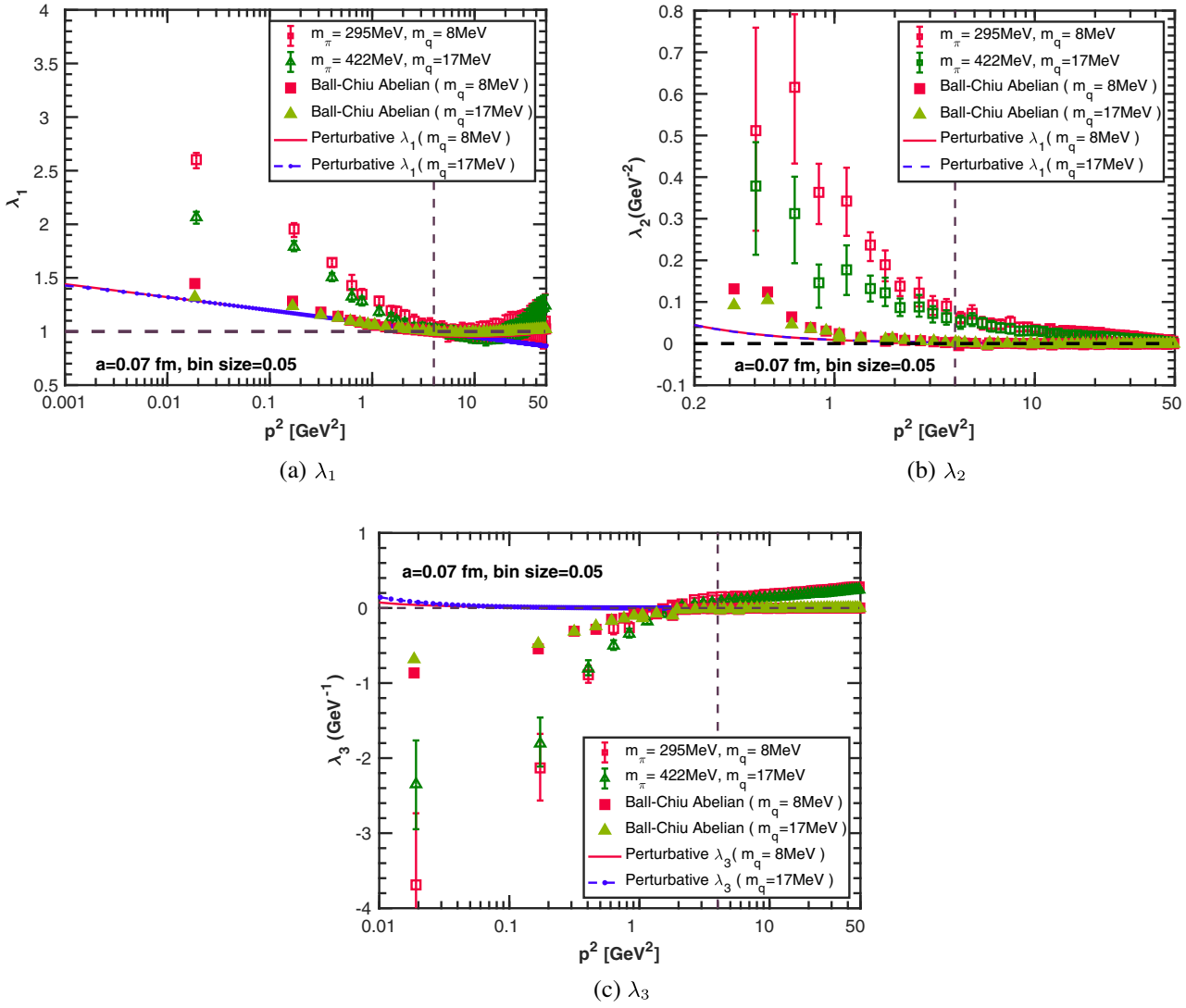

(a) λ_1 (b) λ_2

(c) λ_3

FIG. 10. The form factors λ_1, λ_2, and λ_3 for the L07 ($m_\pi = 295$ MeV) and H07 ($m_\pi = 422$ MeV) ensembles, together with the Abelian Ball-Chiu vertex and the one-loop order form factors, as functions of momentum squared.

Slavnov-Taylor identity (3) show that the Abelian Ball-Chiu vertex is not able to saturate the identity and, therefore, the quark-ghost kernel H in Eq. (3) has sizeable contributions in the infrared region.

C. Mass dependence

In Fig. 10, we show results from the L07 (m_π=295MeV) and H07 ($m_\pi = 422$ MeV) ensembles, which differ only by the quark mass. We also show the corresponding Ball-Chiu vertices and one-loop order perturbative results.

For all form factors we see that the lighter quark mass give rise to a larger infrared enhancement. This is particularly interesting in the case of λ_3, where the one-loop expression (34) increases with increasing quark mass in this momentum region. However, it should be noted that the one-loop expression also shows a stronger enhancement with decreasing quark mass (albeit with the opposite sign) in the deep infrared as shown in Fig. 3(c). We also note that the Abelian Ball-Chiu vertex exhibits the same effect and that the same quark mass dependence was observed for λ_3 in the quenched case [44]. We therefore consider this mass dependence to be robust.

In the case of λ_1 and λ_2, although the one-loop perturbative contribution for the lighter and heavier masses look the same, on closer inspection, one notes that in the deep IR, they differ from each other following the same trend, namely that they are more enhanced the smaller the quark mass is (see Fig. 3).

D. Volume dependence

In Fig. 11, we compare the results for two different volumes with the same quark mass and lattice spacing, $a = 0.07$ fm and $m_\pi = 295$ MeV on the 64^4 and $32^3 \times 64$ lattices, respectively.

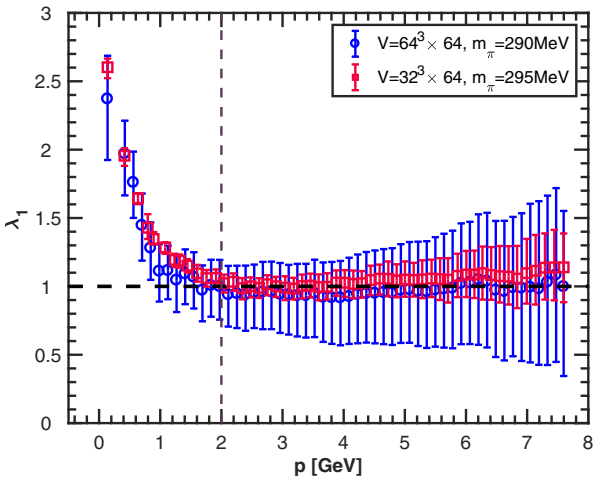

(a) λ_1

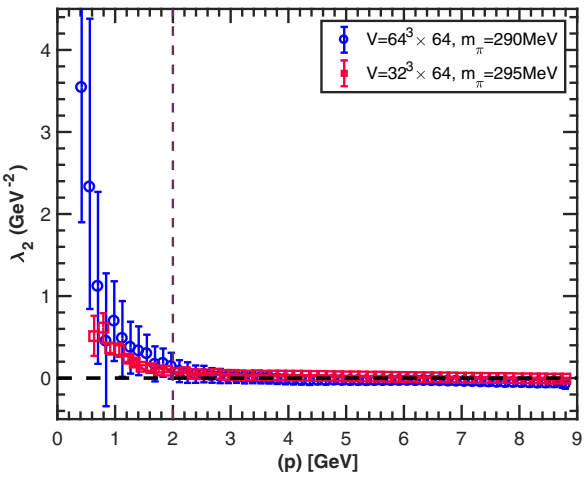

(b) λ_2

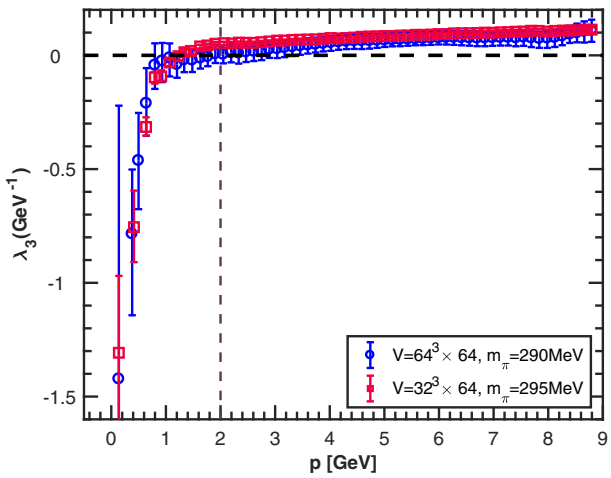

(c) λ_3

FIG. 11. Volume dependence of the form factors λ_1, λ_2, and λ_3, from the L07 and L07-64 ensembles, with $a = 0.07$ fm and $m_\pi \approx 290$ MeV.

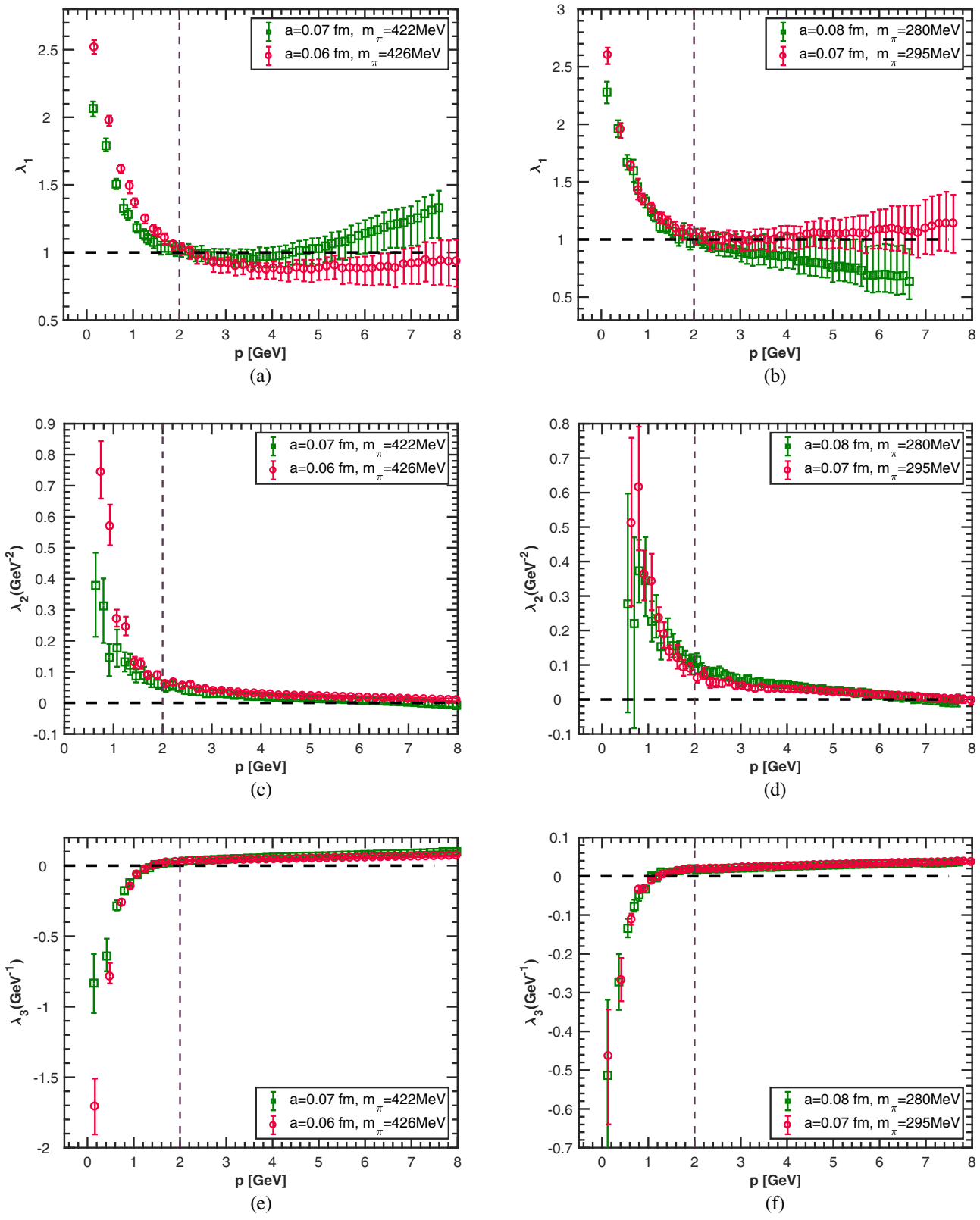

FIG. 12. Lattice spacing dependence of the form factors, for the H06 and H07 (heavier quark) ensembles (left) and the L07 and L08 (lighter quark) ensembles (right).

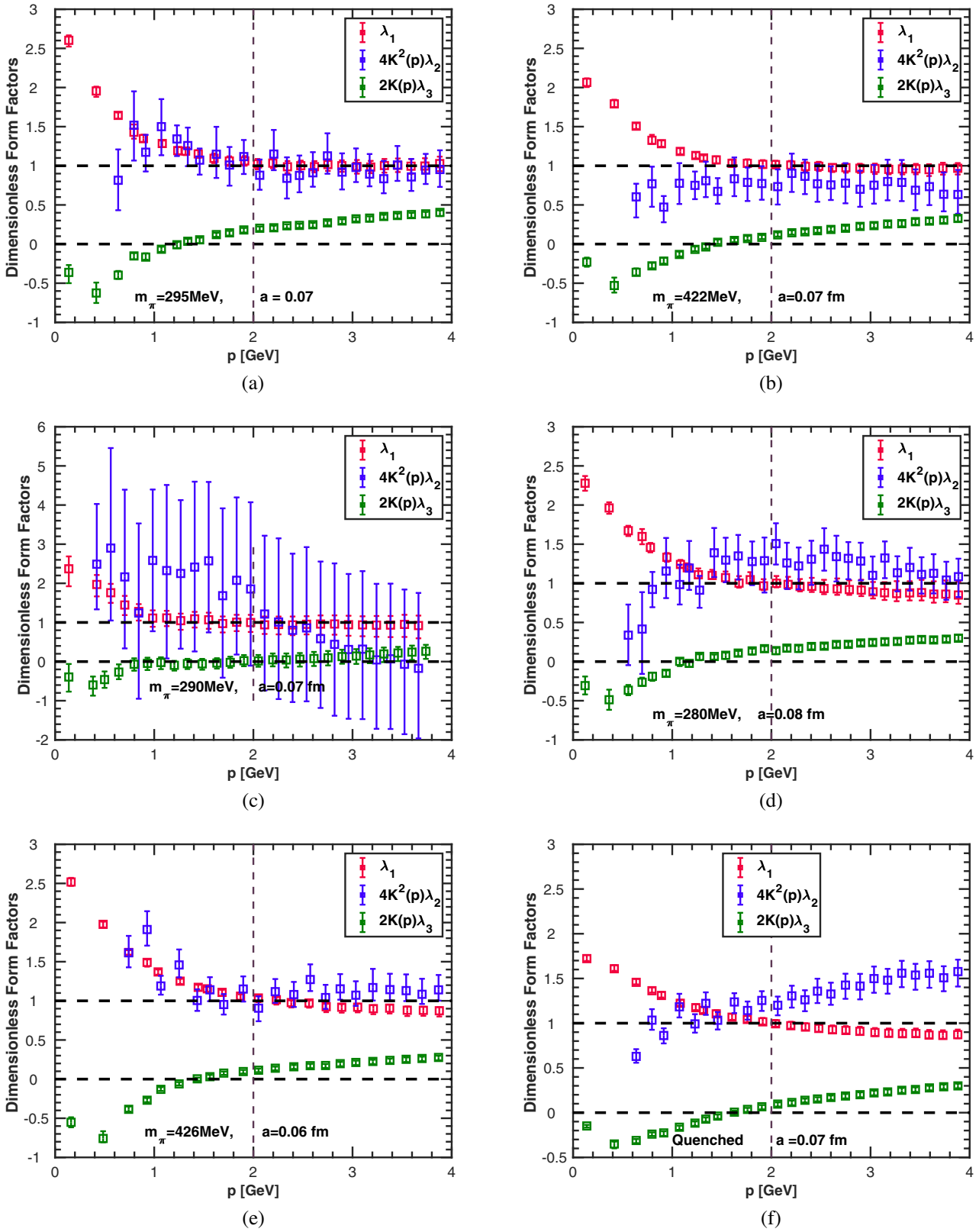

FIG. 13. Dimensionless form factors λ_1, $4K^2(p)\lambda_2$, and $2K(p)\lambda_3$, corresponding in the continuum to λ_1, $4p^2\lambda_2$ and $2p\lambda_3$, for each ensemble versus momentum: (a) ensemble L07, (b) ensemble H07, (c) ensemble L07-64, (d) ensemble L08, (e) ensemble H06, and (f) ensemble Q07. These measure the contribution of each form factor to the strength of the vertex. Note that $K(p)$ and the naive momentum p are equal in the continuum limit.

In all cases, the uncertainties for the larger volume are so large that we are not able to draw any definitive conclusions; however, we do not see any evidence of a significant finite-volume effect for λ_1 or λ_3. For λ_2, our results suggest that this form factor is more strongly enhanced in the infrared as the volume increases; however, the results for the two volumes remain consistent with each other within the uncertainties.

E. Lattice spacing

In Fig. 12, we compare results for different lattice spacings, keeping the quark mass constant. For comparison, in Fig. 12, the plots on the left show results for the H06 and H07 ensembles with $m_\pi \approx 420$ MeV, while the plots on the right are for the L07 and L08 ensembles, with $m_\pi \approx 290$ MeV.

For both quark masses, we observe that all form factors have a larger infrared enhancement for the smaller lattice spacing. The effect is slightly larger for the heavier masses than for the lighter mass.

At large momentum, we see that all form factors move closer to their continuum tree-level value (1 for λ_1 and 0 for λ_2 and λ_3 as the lattice spacing is reduced, suggesting that the expected perturbative behavior will be reproduced in the continuum limit.

F. All form factors

Finally, in Fig. 13, we show all form factors as a function of momentum up to 4 GeV for all lattice ensembles generated for this study. λ_1 is dimensionless, but λ_2 and λ_3 have dimensions of p^{-2} and p^{-1}, respectively. In order to measure the relative strength of λ_2 and λ_3 in comparison to λ_1, all form factors are multiplied by the appropriate lattice momenta. The lattice momentum $K(p)$ is used here to reduce lattice artifacts and ensure the continuum limit is approached more rapidly; note that all momentum variables are equivalent in the continuum limit and that no variable is intrinsically preferred over any other away from the continuum limit.

For all ensembles, regardless of quark mass, volume, and lattice spacing, we find that λ_1 has the biggest contribution to the quark-gluon vertex. The second and third in the hierarchy are the λ_2 and λ_3 form factors, respectively. There is no IR divergence in the soft gluon kinematics, and hence we expect $p^2\lambda_2$ and $p\lambda_3$ to vanish in the deep infrared. Lattice calculations of λ_2 and λ_3 in the deep infrared region are numerically extremely challenging; nevertheless, in all the plots in Fig. 13, we see that their contributions approach zero as $p \to 0$.

IV. CONCLUSIONS AND OUTLOOK

We have performed the first ever study of the quark-gluon vertex in Landau gauge lattice QCD with $N_f = 2$ dynamical fermions. The study has been carried out in the soft gluon limit (gluon momentum $q = 0$), which gives access to three of the nontransverse form factors (λ_1, λ_2, and λ_3).

The quark-gluon vertex is an essential element of QCD, yet its complete nonperturbative form is still unknown. This calculation may be used to calibrate any approximation made for the quark-gluon vertex. Furthermore, it can be used to validate proposed nonperturbative models of the quark-gluon vertex.

We find that the leading form factor λ_1 is significantly enhanced in the infrared and that this enhancement is stronger than in the quenched approximation and increases as the chiral limit is approached. The indications are that the enhancement is further strengthened as the continuum limit is approached. No significant finite-volume effects are found.

The subleading vector form factor λ_2 also exhibits an infrared strength commensurate with, if somewhat smaller than, λ_1. This form factor has only a mild dependence on the number of quark flavors, but the enhancement appears to increase as the continuum, infinite-volume, and chiral limits are approached.

The infrared strength of the scalar form factor λ_3 is considerably larger than in the quenched approximation and also appears to increase as the continuum limit is approached. No significant volume effect is found, but the strength is slightly increased for smaller quark masses. The latter is in contrast to naive expectations as this form factor violates chiral symmetry and is therefore sensitive to the explicit chiral symmetry breaking from the quark mass but suggests that it is primarily governed by the dynamical chiral symmetry breaking.

In all three cases, the nonperturbative effects are found to be orders of magnitude larger than the corresponding one-loop perturbative contributions to these form factors. In all form factors, the lightest masses cause the larger IR enhancement, and it decreases as the mass increases. The dimensionless λ_2 and λ_3 form factors approach zero in the infrared, indicating no kinematic singularities in the soft gluon kinematics.

In the future, we plan to extend this study to general kinematics which will allow us to determine all form factors of the transverse-projected vertex. It is also of interest to compute the vertex in general covariant gauges. Apart from addressing gauge dependence, this would also allow us to disentangle the longitudinal and transverse components, which is not possible in Landau gauge.

ACKNOWLEDGMENTS

The gauge fixing and calculations of the fermion propagators were performed on the HLRN supercomputing facilities in Berlin and Hanover. J. I. S. has been supported by Science Foundation Ireland Grant No. 11/RFP.1/PHY/1362. A. S. acknowledges support by the DFG as member of the projects SFB/TRR55 and GRK1523. O. O. and P. J.

S. acknowledge support from FCT (Portugal) Projects No. UID/FIS/04564/2019 and No. UID/FIS/04564/2020. P. J. S. acknowledges financial support from FCT (Portugal) under Contract No. CEECIND/00488/2017. J. I. S. expresses his deep appreciation for the hospitality of the Centre for the Subatomic Structure of Matter, University of Adelaide, where much of this work was carried out, as well as the Galileo Galilei Institute, Florence, where this work was brought to completion. We thank A. G. Williams for stimulating discussions and support in the early stages of the project. A. K. thanks Professor A. W. Thomas for supporting this work.

APPENDIX: TREE-LEVEL LATTICE EXPRESSIONS

In the following we will make use of the lattice momentum variables defined by

$$\tilde{K}_\nu(p) = \frac{1}{2a}\sin 2p_\nu a, \tag{A1}$$

$$K_\nu(p) = \frac{1}{a}\sin p_\nu a, \tag{A2}$$

$$Q_\nu(p) = \frac{2}{a}\sin\left(\frac{p_\nu a}{2}\right), \tag{A3}$$

$$C_\nu(p) = \cos(p_\nu a), \tag{A4}$$

$$\bar{C}_\nu(p) = \cos\left(\frac{p_\nu a}{2}\right). \tag{A5}$$

In terms of these variables, the tree-level quark–gluon vertex in Eq. (21) can be rewritten as

$$\bar{\Lambda}^{(0)}_{0,\nu}(p,q,k) = (-ig_0)\left\{\gamma_\nu a\bar{C}_\nu(p+k) - \frac{i}{2}aQ_\nu(p+k)\boldsymbol{I} - i\frac{c_{\rm SW}}{2}a\bar{C}_\nu(q)\sum_\lambda \sigma_{\nu\lambda}aK_\lambda(q)\right\}, \tag{A6}$$

for the case of the 'unimproved' propagator $S_0(x,y) = \langle\psi(x)\bar{\psi}(y)\rangle$. The improved vertex obtained using the rotated propagator (6) is given at tree level by

$$\bar{\Lambda}^{(0)}_{R,\nu}(p,q,k) = (1+b_q am)[S^{(0)}_R(p)]^{-1}S^{(0)}_0(p)[\Lambda^{a(0)}_{0,\nu}(p,q,k)] \times S^{(0)}_0(k)[S^{(0)}_R(k)]^{-1}, \tag{A7}$$

where $S^{(0)}_0(p)$ is the tree-level, unimproved, dimensionless Wilson quark propagator, while $S^{(0)}_R(p)$ is the level expression for the improved propagator (6), given by [50]

$$S^{(0)}_0(p) = \frac{1}{D}\left[-ia\not{K}(p) + ma + \frac{1}{2}a^2Q^2(p)\right], \tag{A8}$$

$$S^{(0)}_R(p)^{-1} = \frac{D}{(1+ma/2)D_R}(ia\not{K}(p)A_R + B_R), \tag{A9}$$

where

$$D = a^2K^2(p) + \left(ma + \frac{1}{2}a^2Q^2(p)\right)^2, \tag{A10}$$

$$D_R = a^2K^2(p)A_R^2 + B_R^2, \tag{A11}$$

$$A_R = 1 + \frac{1}{2}am + \frac{1}{4}a^2Q^2(p) - \frac{1}{16}a^2K^2(p), \tag{A12}$$

$$B_R = \left(am + \frac{1}{2}a^2Q^2(p)\right)\left(1 - \frac{a^2K^2(p)}{16}\right) - \frac{1}{2}a^2K^2(p), \tag{A13}$$

Making use of the tree-level unimproved (A8) and the rotated-improved (A9) propagators in Eq. (A7), the tree-level quark-gluon vertex can be rewritten as

$$\bar{\Lambda}^{(0)}_{R,\nu}(p,q) = \frac{(1+b_q am)}{(1+am/2)^2D_R(p)D_R(k)} \times [-ia\not{K}(p)A^R_V(p) + B^R_V(p)][\Lambda^{a(0)}_{0,\nu}(p,q,k)] \times [-ia\not{K}(k)A^R_V(k) + B^R_V(k)], \tag{A14}$$

where

$$A^R_V(p) = 2c_qD(p), \tag{A15}$$

$$B^R_V(p) = (1 - c_q^2a^2K^2(p))D^2(p), \tag{A16}$$

$$D^2_R(p) = \left(1 + \frac{a^2K^2(p)}{16}\right)^2D(p). \tag{A17}$$

and after further manipulation we arrive at the expression

$$\bar{\Lambda}^{(0)}_{R,\nu}(p,q,k) = \frac{(1+b_q am)}{(1+am/2)^2}\frac{D(p)D(k)}{D_R(p)D_R(k)} \times [2ic_qa\not{K}(p) + 1 - c_q^2a^2K^2(p)] \times [\Lambda^{a(0)}_{0,\nu}(p,q,k)] \times [2ic_qa\not{K}(k) + 1 - c_q^2a^2K^2(k)]. \tag{A18}$$

As discussed above [see Eq. (9)], for $q \neq 0$ we can only access the transverse vertex on the lattice in the Landau gauge. Hence, using the lattice equivalent of the transverse projector, $P^T_{\mu\nu} = \sum_\nu(\delta_{\mu\nu} - \frac{K_\mu(q)K_\nu(q)}{K^2(q)})$, the tree-level quark-gluon vertex in general kinematics is given by

$$\begin{aligned}\bar{\Lambda}^{(0)}_{R,\mu}(p,q,k) &= P^T_{\mu\nu}(q)\Lambda^{(0)}_{R,\nu}(p,q,k)\\ &= \frac{(1+b_q am)}{(1+am/2)^2}\frac{1}{(1+c_q^2a^2K^2(p))^2(1+c_q^2a^2K^2(k))^2}\\ &\times\sum_\nu\left(\delta_{\mu\nu}-\frac{K_\mu(q)K_\nu(q)}{K^2(q)}\right)[2ic_q a\not{K}(p)+1-c_q^2a^2K^2(p)][\Lambda^{a(0)}_{0,\nu}(p,q,k)]\\ &\times[2ic_q a\not{K}(k)+1-c_q^2a^2K^2(k)].\end{aligned}\tag{A19}$$

The general form of the tree-level clover-rotated vertex (A19) is highly complicated. However, it simplifies in the soft-gluon kinematics which is the case we are studying in this paper. In this kinematics the gluon momentum $q=0$ and both the quark momenta are equal, $k=p$. In this case the 'unimproved' tree-level vertex (A6) becomes

$$\begin{aligned}\bar{\Lambda}^{(0)}_{0,\nu}(p,0,p) &= -ig_0\left(\boldsymbol{\gamma}_\nu\bar{C}_\nu(2p)-\frac{i}{2}aQ_\nu(2p)\boldsymbol{I}\right)\\ &= -ig_0(\boldsymbol{\gamma}_\nu C_\nu(p)-iaK_\nu(p)\boldsymbol{I}),\end{aligned}\tag{A20}$$

and the tree-level clover-rotated vertex (A19) reduces to

$$\begin{aligned}\bar{\Lambda}^{(0)}_{R,\mu}(p,0,p) &= (-ig_0)F(p)[2ic_q a\not{K}(p)+1-c_q^2a^2K^2(p)]\\ &\times[\Lambda^{a(0)}_{0,\mu}(p,0)]\\ &\times[2ic_q a\not{K}(p)+1-c_q^2a^2K^2(p)],\end{aligned}\tag{A21}$$

where the common prefactor $F(p)$ is given by

$$F(p)=\frac{(1+b_q am)}{(1+am/2)^2}\frac{1}{(1+c_q^2a^2K^2(p))^4}.\tag{A22}$$

After rearranging Eq. (A21) to match the form of Eq. (12), the final shape of the tree-level clover-rotated quark-gluon vertex in the soft gluon kinematics is

$$\begin{aligned}\bar{\Lambda}^{(0)}_{R,\mu}(p,0,p) &= (-ig_0)\frac{(1+b_q am)}{(1+am/2)^2}\frac{1}{(1+c_q^2a^2K^2(p))^4}\\ &\times\Big\{\boldsymbol{\gamma_\mu}[(1+c_q^2a^2K^2(p))^2C_\mu(p)]-\boldsymbol{4a^2K_\mu\not{K}(p)}[-c_q(1-c_q^2a^2K^2(p))+2c_q^2C_\mu(p)]\\ &-\boldsymbol{2iaK_\mu}\left[-2c_q^2a^2K^2(p)+\frac{1}{2}(1-c_q^2a^2K^2(p))-2c_q(1-c_q^2a^2K^2(p))C_\mu(p)\right]\Big\}.\end{aligned}\tag{A23}$$

Making a comparison between this expression and the continuum vertex Eq. (12), we can identify the tree-level expressions for the form factors in the soft-gluon kinematics:

$$\lambda_1^{(0)}+\bar{\lambda}^{(0)}_{1(\mu)}=F(p)[(1+c_q^2a^2K^2(p))^2C_\mu(p)]|_{p_\mu=0}=\frac{(1+b_q am)}{(1+am/2)^2}\frac{1}{(1+c_q^2a^2K^2(p))^2},\tag{A24}$$

$$\lambda_2^{(0)}+\bar{\lambda}^{(0)}_{2(\mu)}=a^2F(p)[-c_q(1-c_q^2a^2K^2(p))+2c_q^2C_\mu(p)],\tag{A25}$$

$$\lambda_3^{(0)}+\bar{\lambda}^{(0)}_{3(\mu)}=aF(p)\left[-2c_q^2a^2K^2(p)+\frac{1}{2}(1-c_q^2a^2K^2(p))^2-2c_q(1-c_q^2a^2K^2(p))C_\mu(p)\right].\tag{A26}$$

We note in particular that there are two separate tensor structures appearing in the tree-level vertex (A23) which in the continuum become equal to $L_{2,\mu}$, and likewise for $L_{3,\mu}$. In Eqs (A25) and (A26) these are associated with separate form factors $\lambda_i^{(0)}$ and $\bar{\lambda}_i^{(0)}$ respectively.

Inspecting Eq. (A23) and comparing this with the continuum expressions (18), (19), (17), we can write down the lattice equivalents of these expressions, namely

$$\lambda_1(p^2,0,p^2) = \frac{1}{(-ig_0)}\left\{[\mathrm{Tr}_4(\gamma_\alpha\bar{\Lambda}_\mu)]|_{\substack{\alpha=\mu\\ p_\mu=0}}\right\} = \frac{\mathbf{Im}}{g_0}\left\{[\mathrm{Tr}_4(\gamma_\alpha\bar{\Lambda}_\mu)]|_{\substack{\alpha=\mu\\ p_\mu=0}}\right\}, \tag{A27}$$

$$\begin{aligned}\lambda_2(p^2,0,p^2) &= \frac{1}{(-ig_0)}\left\{-\frac{1}{4K(p)^2}\frac{K_\alpha(p)K_\mu(p)}{K(p)^2}[\mathrm{Tr}_4(\gamma_\alpha\bar{\Lambda}_\mu)|_{\alpha\neq\mu}]\right\}\\ &= \frac{\mathbf{Im}}{g_0}\left\{-\frac{1}{4K(p)^2}\frac{K_\alpha(p)K_\mu(p)}{K(p)^2}[\mathrm{Tr}_4(\gamma_\alpha\bar{\Lambda}_\mu)|_{\alpha\neq\mu}]\right\},\end{aligned} \tag{A28}$$

$$\lambda_3(p^2,0,p^2) = \frac{1}{(-ig_0)}\left\{\frac{i}{2}\frac{K_\mu(p)}{K^2(p)}\mathrm{Tr}_4(I\bar{\Lambda}_\mu)\right\} = \frac{\mathbf{Re}}{(-g_0)}\left\{\frac{1}{2}\frac{K_\mu(p)}{K^2(p)}\mathrm{Tr}_4(I\bar{\Lambda}_\mu)\right\}. \tag{A29}$$

Although Eq. (A29) is based on the covariant expression (17), we will in practice not sum over μ in Eq. (A29), just as there is no sum over μ and α in Eqs (A27) and (A28). Combining this with the tree-level form factors, Eqs (A24), (A25), (A26), we arrive at the expressions we will use to determine the tree-level corrected form factors λ_i in the soft gluon kinematics,

$$\lambda_1(p^2,0,p^2) = \frac{\mathbf{Im}}{g_0}\left\{[\mathrm{Tr}_4(\gamma_\alpha\bar{\Lambda}_\mu)]|_{\substack{\alpha=\mu\\ p_\mu=0}}\right\}\Big/\lambda_1^{(0)}, \tag{A30}$$

$$\lambda_2(p^2,0,p^2) = \frac{\mathbf{Im}}{g_0}\left\{-\frac{1}{4K(p)^2}\frac{K_\alpha(p)K_\mu(p)}{K(p)^2}[\mathrm{Tr}_4(\gamma_\alpha\bar{\Lambda}_\mu)|_{\alpha\neq\mu}]\right\} - (\lambda_2^{(0)} + \bar{\lambda}_{2(\mu)}^{(0)}), \tag{A31}$$

$$\lambda_3(p^2,0,p^2) = \frac{\mathbf{Re}}{(-g_0)}\left\{\frac{1}{2}\frac{K_\mu(p)}{K^2(p)}\mathrm{Tr}_4(I\bar{\Lambda}_\mu)\right\} - (\lambda_3^{(0)} + \bar{\lambda}_{3(\mu)}^{(0)}). \tag{A32}$$

These (λ_1, λ_2, λ_3) are the complete form factors required to determine the quark-gluon vertex in the soft gluon limits and Eqs (A30), (A31), (A32)define the exact procedures to calculate them on the lattice.

For completeness and future reference, we also include the tree-level lattice equivalents of the covariant expressions (15)–(17),

$$\sum_\mu \mathrm{Tr}_4(\gamma_\mu\bar{\Lambda}_\mu^{R(0)}(p,0)) = F(p)\left([(1-c_q^2K^2(p))^2+4c_q^2K^2(p)]\left(4-\frac{1}{2}Q^2(p)\right)+4c_q(1-c_q^2K^2(p))K^2(p)-8c_q^2K(p)\cdot\tilde{K}(p)\right) \tag{A33}$$

$$\sum_{\alpha\mu} K_\alpha(p)K_\mu(p)\mathrm{Tr}_4(\gamma_\alpha\bar{\Lambda}_\mu^{R(0)}(p,0)) = F(p)\left([(1-c_q^2K^2(p))^2-4c_q^2K^2(p)]K(p)\cdot\tilde{K}(p)+c_q(1-c_q^2K^2(p))(K^2(p))^2\right) \tag{A34}$$

$$\sum_\mu \frac{K_\mu(p)}{K^2(p)}\mathrm{Tr}_4(\bar{\Lambda}_\mu^{R(0)}(p,0)) = -\frac{iF(p)}{2}\left[(1-c_q^2K^2(p))^2-4c_q^2K^2(p)-4c_q(1-c_q^2K^2(p))\frac{K(p)\cdot\tilde{K}(p)}{K^2(p)}\right] \tag{A35}$$

$$\lambda_{1,\mathrm{cov}}^{(0)} = \frac{1}{3}\left[(\mathrm{A34})-\frac{(\mathrm{A35})}{K^2(p)}\right] = \frac{F(p)}{3}\left[4-\frac{1}{2}Q^2(p)-\frac{K(p)\cdot\tilde{K}(p)}{K^2(p)}\right][(1-c_q^2K^2(p))^2+4c_q^2K^2(p)] \tag{A36}$$

$$\begin{aligned}\lambda_{2,\mathrm{cov}}^{(0)} &= \frac{1}{12K^2(p)}\left[(\mathrm{A34})-4\frac{(\mathrm{A35})}{K^2(p)}\right]\\ &= F(p)\left(\frac{(1-c_q^2K^2(p))^2}{3K^2(p)}\left[1-\frac{K(p)\cdot\tilde{K}(p)}{K^2(p)}-\frac{1}{8}Q^2(p)\right]-c_q(1-c_q^2K^2(p))+\frac{4c_q^2}{3}\left[1+\frac{K(p)\cdot\tilde{K}(p)}{2K^2(p)}-\frac{1}{8}Q^2(p)\right]\right)\end{aligned} \tag{A37}$$

[1] A. Kızılersü, T. Sizer, and A. G. Williams, Strongly-coupled unquenched QED_4 propagators using Schwinger–Dyson equations, Phys. Rev. D **88**, 045008 (2013).

[2] P. Maris, C. D. Roberts, and P. C. Tandy, Pion mass and decay constant, Phys. Lett. B **420**, 267 (1998).

[3] P. Maris and P. C. Tandy, Bethe-Salpeter study of vector meson masses and decay constants, Phys. Rev. C **60**, 055214 (1999).

[4] P. Maris and P. C. Tandy, The π, K^+, and K^0 electromagnetic form-factors, Phys. Rev. C **62**, 055204 (2000).

[5] L. Chang, I. C. Cloët, C. D. Roberts, S. M. Schmidt, and P. C. Tandy, Pion Electromagnetic Form Factor at Spacelike momenta, Phys. Rev. Lett. **111**, 141802 (2013).

[6] A. Bashir, R. Bermudez, L. Chang, and C. D. Roberts, Dynamical chiral symmetry breaking and the fermion–gauge-boson vertex, Phys. Rev. C **85**, 045205 (2012).

[7] L. Chang, I. C. Cloet, J. J. Cobos-Martinez, C. D. Roberts, S. M. Schmidt, and P. C. Tandy, Imaging Dynamical Chiral Symmetry Breaking: Pion Wave Function on the Light Front, Phys. Rev. Lett. **110**, 132001 (2013).

[8] L. Chang and C. D. Roberts, Sketching the Bethe-Salpeter Kernel, Phys. Rev. Lett. **103**, 081601 (2009).

[9] A. Maas, Describing gauge bosons at zero and finite temperature, Phys. Rep. **524**, 203 (2013).

[10] A. Sternbeck and L. von Smekal, Infrared exponents and the strong-coupling limit in lattice Landau gauge, Eur. Phys. J. C **68**, 487 (2010).

[11] A. Sternbeck and M. Müller-Preussker, Lattice evidence for the family of decoupling solutions of Landau gauge Yang–Mills theory, Phys. Lett. B **726**, 396 (2013).

[12] O. Oliveira, A. G. Duarte, D. Dudal, and P. J. Silva, Gluon and ghost dynamics from lattice QCD, Few Body Syst. **58**, 99 (2017).

[13] A. G. Duarte, O. Oliveira, and P. J. Silva, Lattice gluon and ghost propagators, and the strong coupling in pure SU(3) Yang-Mills theory: Finite lattice spacing and volume effects, Phys. Rev. D **94**, 014502 (2016).

[14] M. B. Parappilly, P. O. Bowman, U. M. Heller, D. B. Leinweber, A. G. Williams, and J. B. Zhang, Scaling behavior of quark propagator in full QCD, Phys. Rev. D **73**, 054504 (2006).

[15] W. Kamleh, P. O. Bowman, D. B. Leinweber, A. G. Williams, and J. Zhang, Unquenching effects in the quark and gluon propagator, Phys. Rev. D **76**, 094501 (2007).

[16] O. Oliveira, P. J. Silva, J.-I. Skullerud, and A. Sternbeck, Quark propagator with two flavors of O(a)-improved Wilson fermions, Phys. Rev. D **99**, 094506 (2019).

[17] C. S. Fischer, Infrared properties of QCD from Dyson–Schwinger equations, J. Phys. G **32**, R253 (2006).

[18] D. Binosi and J. Papavassiliou, Pinch technique: Theory and applications, Phys. Rep. **479**, 1 (2009).

[19] J. Braun, L. Fister, J. M. Pawlowski, and F. Rennecke, From quarks and gluons to hadrons: Chiral symmetry breaking in dynamical QCD, Phys. Rev. D **94**, 034016 (2016).

[20] A. K. Cyrol, M. Mitter, J. M. Pawlowski, and N. Strodthoff, Nonperturbative quark, gluon, and meson correlators of unquenched QCD, Phys. Rev. D **97**, 054006 (2018).

[21] A. C. Aguilar, F. De Soto, M. N. Ferreira, J. Papavassiliou, J. Rodríguez-Quintero, and S. Zafeiropoulos, Gluon propagator and three-gluon vertex with dynamical quarks, Eur. Phys. J. C **80**, 154 (2020).

[22] M. S. Bhagwat and P. C. Tandy, Quark-gluon vertex model and lattice-QCD data, Phys. Rev. D **70**, 094039 (2004).

[23] A. Kızılersü and M. R. Pennington, Building the full fermion-photon vertex of QED by imposing multiplicative renormalizability of the Schwinger-Dyson equations for the fermion and photon propagators, Phys. Rev. D **79**, 125020 (2009).

[24] L. Chang, Y.-X. Liu, and C. D. Roberts, Dressed-Quark Anomalous Magnetic Moments, Phys. Rev. Lett. **106**, 072001 (2011).

[25] M. Mitter, J. M. Pawlowski, and N. Strodthoff, Chiral symmetry breaking in continuum QCD, Phys. Rev. D **91**, 054035 (2015).

[26] A. C. Aguilar, D. Binosi, D. Ibañez, and J. Papavassiliou, New method for determining the quark-gluon vertex, Phys. Rev. D **90**, 065027 (2014).

[27] A. C. Aguilar, J. C. Cardona, M. N. Ferreira, and J. Papavassiliou, Non-abelian Ball–Chiu vertex for arbitrary euclidean momenta, Phys. Rev. D **96**, 014029 (2017).

[28] D. Binosi, L. Chang, J. Papavassiliou, S.-X. Qin, and C. D. Roberts, Natural constraints on the gluon-quark vertex, Phys. Rev. D **95**, 031501(R) (2017).

[29] R. Bermudez, L. Albino, L. X. Gutiérrez-Guerrero, M. E. Tejeda-Yeomans, and A. Bashir, Quark-gluon vertex: A perturbation theory primer and beyond, Phys. Rev. D **95**, 034041 (2017).

[30] A. Kızılersü, T. Sizer, M. R. Pennington, A. G. Williams, and R. Williams, Dynamical mass generation in unquenched QED using the Dyson–Schwinger equations, Phys. Rev. D **91**, 065015 (2015).

[31] R. Williams, The quark-gluon vertex in Landau gauge bound-state studies, Eur. Phys. J. A **51**, 57 (2015).

[32] O. Oliveira, T. Frederico, W. de Paula, and J. P. B. C. de Melo, Exploring the quark-gluon vertex with Slavnov–Taylor identities and lattice simulations, Eur. Phys. J. C **78**, 553 (2018).

[33] O. Oliveira, T. Frederico, and W. de Paula, The soft-gluon limit and the infrared enhancement of the quark-gluon vertex, Eur. Phys. J. C **80**, 484 (2020).

[34] F. E. Serna, C. Chen, and B. El-Bennich, Interplay of dynamical and explicit chiral symmetry breaking effects on a quark, Phys. Rev. D **99**, 094027 (2019).

[35] F. Gao, J. Papavassiliou, and J. M. Pawlowski, Fully coupled functional equations for the quark sector of QCD, Phys. Rev. D **103**, 094013 (2021).

[36] R. Williams, C. S. Fischer, and W. Heupel, Light mesons in QCD and unquenching effects from the 3PI effective action, Phys. Rev. D **93**, 034026 (2016).

[37] M. Atif Sultan, F. Akram, B. Masud, and K. Raya, Effect of the quark-gluon vertex on dynamical chiral symmetry breaking, Phys. Rev. D **103**, 054036 (2021).

[38] A. C. Aguilar, J. C. Cardona, M. N. Ferreira, and J. Papavassiliou, Quark gap equation with non-abelian Ball–Chiu vertex, Phys. Rev. D **98**, 014002 (2018).

[39] H.-X. He, F. C. Khanna, and Y. Takahashi, Transverse Ward–Takahashi identity for the fermion boson vertex in gauge theories, Phys. Lett. B **480**, 222 (2000).
[40] K.-I. Kondo, Transverse Ward–Takahashi identity, anomaly and Schwinger–Dyson equation, Int. J. Mod. Phys. A **12**, 5651 (1997).
[41] M. R. Pennington and R. Williams, Checking the transverse Ward-Takahashi relation at one loop order in 4-dimensions, J. Phys. G **32**, 2219 (2006).
[42] H.-x. He, Transverse symmetry transformations and the quark-gluon vertex function in QCD, Phys. Rev. D **80**, 016004 (2009).
[43] J.-I. Skullerud and A. Kızılersü, Quark-gluon vertex from lattice QCD, J. High Energy Phys. 09 (2002) 013.
[44] J.-I. Skullerud, P. O. Bowman, A. Kızılersü, D. B. Leinweber, and A. G. Williams, Nonperturbative structure of the quark gluon vertex, J. High Energy Phys. 04 (2003) 047.
[45] A. Kızılersü, D. B. Leinweber, J.-I. Skullerud, and A. G. Williams, Quark-gluon vertex in general kinematics, Eur. Phys. J. C **50**, 871 (2007).
[46] M. Peláez, M. Tissier, and N. Wschebor, Quark-gluon vertex from the Landau gauge Curci-Ferrari model, Phys. Rev. D **92**, 045012 (2015).
[47] O. Oliveira, A. Kızılersü, P. J. Silva, J.-I. Skullerud, A. Sternbeck, and A. G. Williams, Lattice Landau gauge quark propagator and the quark-gluon vertex, Acta Phys. Pol. B Proc. Suppl. **9**, 363 (2016).
[48] A. Sternbeck, P.-H. Balduf, A. Kızılersü, O. Oliveira, P. J. Silva, J.-I. Skullerud, and A. G. Williams, Triple-gluon and quark-gluon vertex from lattice QCD in Landau gauge, Proc. Sci., LATTICE2016 (**2017**) 349 [arXiv:1702.00612].
[49] J. I. Skullerud and A. G. Williams, Quark propagator in the Landau gauge, Phys. Rev. D **63**, 054508 (2001).
[50] J.-I. Skullerud, D. B. Leinweber, and A. G. Williams, Nonperturbative improvement and tree-level correction of the quark propagator, Phys. Rev. D **64**, 074508 (2001).
[51] J. S. Ball and T.-W. Chiu, Analytic properties of the vertex function in gauge theories. 1. Phys. Rev. D **22**, 2542 (1980).
[52] A. Kızılersü, M. Reenders, and M. R. Pennington, One loop QED vertex in any covariant gauge: Its complete analytic form, Phys. Rev. D **52**, 1242 (1995).
[53] B. Sheikholeslami and R. Wohlert, Improved continuum limit lattice action for QCD with Wilson fermions, Nucl. Phys. **B259**, 572 (1985).
[54] S. Capitani *et al.*, Renormalisation and off-shell improvement in lattice perturbation theory, Nucl. Phys. **B593**, 183 (2001).
[55] G. S. Bali *et al.*, Nucleon mass and sigma term from lattice QCD with two light fermion flavors, Nucl. Phys. **B866**, 1 (2013).
[56] G. S. Bali, S. Collins, B. Gläßle, M. Göckeler, J. Najjar, R. H. Rödl, A. Schäfer, R. W. Schiel, A. Sternbeck, and W. Söldner, The moment $\langle x \rangle_{u-d}$ of the nucleon from $N_f = 2$ lattice QCD down to nearly physical quark masses, Phys. Rev. D **90**, 074510 (2014).
[57] G. S. Bali, S. Collins, B. Gläßle, M. Göckeler, J. Najjar, R. H. Rödl, A. Schäfer, R. W. Schiel, W. Söldner, and A. Sternbeck, Nucleon isovector couplings from $N_f = 2$ lattice QCD, Phys. Rev. D **91**, 054501 (2015).
[58] $\lambda_4 = 0$ in this kinematics because of charge conjugation symmetry, which dictates that $\lambda_4(p^2,q^2,k^2) = -\lambda_4(k^2,q^2,p^2)$.
[59] G. Heatlie, G. Martinelli, C. Pittori, G. C. Rossi, and C. T. Sachrajda, The improvement of hadronic matrix elements in lattice QCD, Nucl. Phys. **B352**, 266 (1991).
[60] S. Capitani and G. Rossi, Deep inelastic scattering in improved lattice QCD. 1. The first moment of structure functions, Nucl. Phys. **B433**, 351 (1995).
[61] S. Bethke, The 2009 world average of α_s, Eur. Phys. J. C **64**, 689 (2009).
[62] S. Bethke, G. Dissertori, and G. P. Salam, World summary of α_s (2015), EPJ Web Conf. **120**, 07005 (2016).